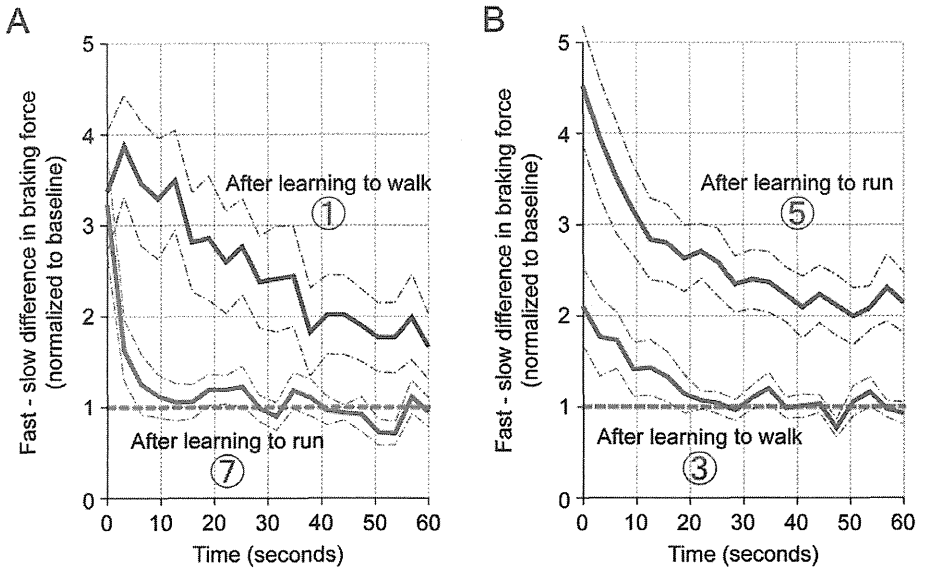

Figure 4. Degree of transfer in the acquired movement pattern across walking and running, shown as differences in the peak braking force between the sides. The extent of asymmetry in (A) walking after adaptation to walk (first washout period in Experiment 1, darker line) and after adaptation to run (first washout period in Experiment 4, lighter line), and (B) running after adaptation to run (first washout period in Experiment 3, darker line) and after adaptation to run (first washout period in Experiment 2, lighter line). Data are normalized to the mean of those during the baseline on a subject-to-subject basis and are presented as the mean (thick line) and the standard errors of the mean (dotted lines).
doi:10.1371/journal.pone.0046349.g004

respective modes were rarely washed out by the subsequent execution in the opposite modes, again, for both directions. That is, the storage of a learned movement patterns were maintained independently of the opposite mode. Combined, these results demonstrated only partially overlapped elements between these two movement modes and thus support the notion of mostly independent functional networks within the CNS for the respective locomotive modes. Walking and running, therefore, reflect not only functions of different speeds of locomotion, but are different forms from the perspective of neural control mechanisms.

The notion of task-specific or context-specific neural mechanisms has been well established by using simple reaching movements in the upper extremities [9,10]. Locomotive movements that are more complex and autonomic have also been found as under the specificity, such as the direction (forward-backward) [11], the limb (right-left) [11], and the speed of walking [12]. Limitations in the transfer or washout in newly acquired movement patterns under certain physical constraints in one movement tasks to or by another have been accepted as indirect evidence demonstrating the specificity [9–12]. By adopting the well-established experimental paradigms in the earlier studies, the present study is the first to address the mode-specificity, comprising an important aspect of locomotion. Because of the well-known spontaneous behavior to transit into the opposite mode (walk-run or run-walk transition) in accordance with changing speed [2,6–8], walking and running may only be considered as a function of demands for different speeds.

The use of split-treadmill walking to modify gait symmetry has been studied extensively in the last decade [11,12,6]. After walking on an asymmetrically-driven treadmill for a certain period of time, the movement pattern after release from the novel environment resulted in prominent asymmetry [11,12,16]. The current study, for the first time, demonstrated that movement patterns in running also could be modified as in the earlier studies focusing on walking. Detailed explanations on how the gait patterns could be adapted with exposure to the asymmetrically driven treadmill and resulted in the subsequent aftereffect have been provided previously both behaviorally and mathematically on the basis of locomotion in decerebrate cat [18].

In the present study, the modification in the gait patterns was most evident in the anterior braking component of the ground reaction force both in walking and running and we therefore focused on this parameter (detailed description in the Methods). As subjects adapted to walk or run comfortably on the asymmetrically driven treadmill, the patterns of modification in the anterior braking force showed gradual increment in the fast side and decrement in the slow side, both including brief and more rapid changes in the early phases of exposure. As a consequence, with return to the symmetrical belt in the washout period, there was initially an overshoot in the force in the fast side and an undershoot for the slow side, both followed by gradual decay into the opposite direction to those during the adaptation periods (towards baseline). Combined with results in a previous study in which novel motor pattern could be stored intralimb and independently for each leg [11], these phenomena occurring for the each limb may reflect the well-established notion of motor adaptation or learning where motor output is recalibrated to meet new task demands [19]. It is reasonable to consider that the asymmetry in the anterior braking force took place based on the recalibration of motor output in each leg under different velocity on an asymmetrically driven treadmill.

The motor output acquired through the above mentioned recalibration processes, however, were only partially shared across the movement modes. Given the results, with the possibility of specificity in the neural mechanisms underlying walking and running, the discussion will now focus on the possible neural mechanisms comprising the different modes. Based on the results of animal studies and of humans, the neural mechanisms underlying the present results could be attributed to possible contribution of supraspinal structures in the brain and the

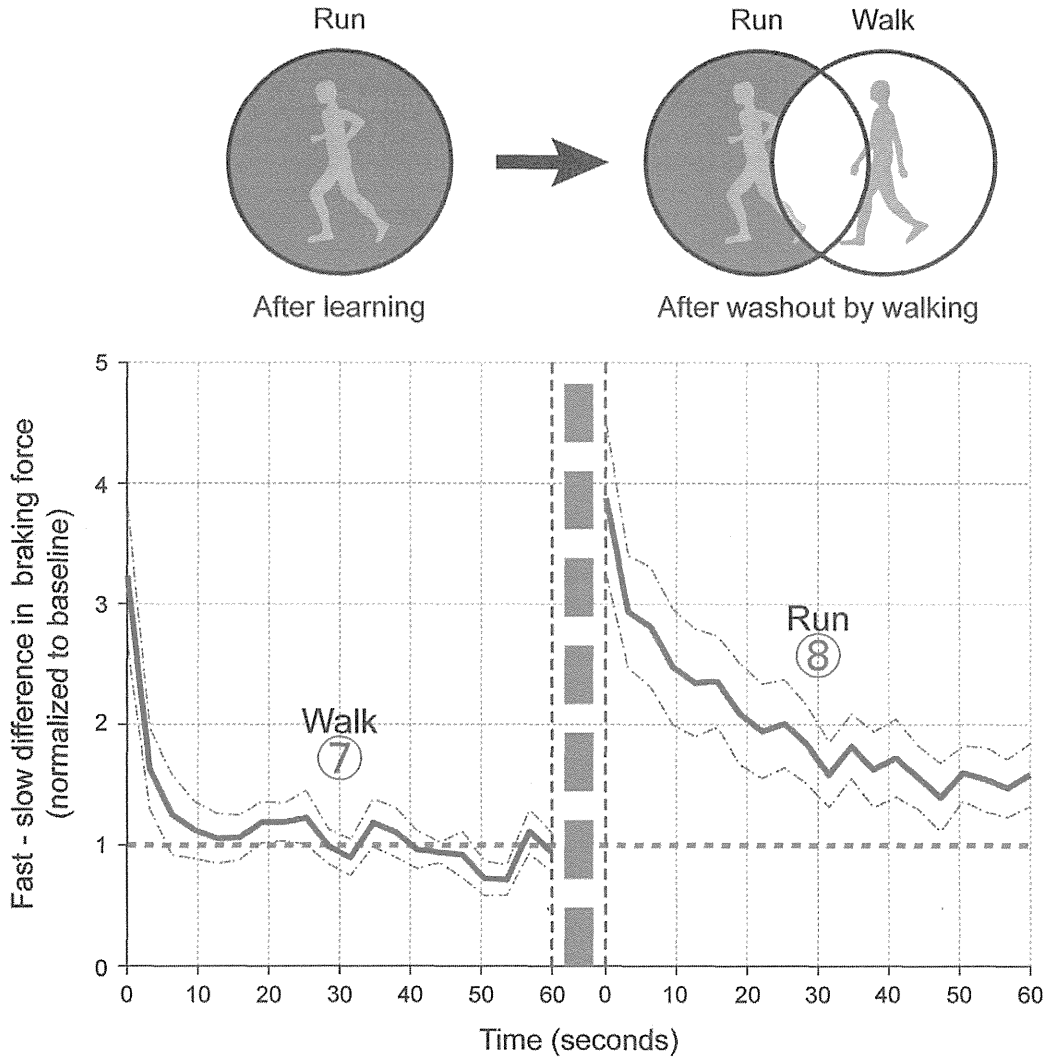

Figure 5. Degree of washout in the stored motor pattern in running by walking (first and second washout periods shown consecutively from Experiment 4). The asymmetrical movement pattern was evident with the initiation of running (red lines) despite a symmetrical walking pattern at the end of the first washout period in walking (blue lines), an indication of only partial washout (also described in the schematic figure). Data are presented as means (thick lines) and their standard errors of the mean (dotted lines).
doi:10.1371/journal.pone.0046349.g005

specificity in the locomotor center in the spinal cord, known as the central pattern generator (CPG).

First, in the emergence of the adaptive phenomena, the cerebellum is considered to play a significant role by recalibrating motor output that satisfies the task or environmental demand [20]. Given its function, any aspect of an aftereffect following adaptation is abolished in humans [17] and in cats [21] with cerebellar lesions. Morton et al. (2006) [17] reported that a predictive feedforward motor adaptation in splitbelt treadmill walking that is demonstrated to occur in healthy subjects [11,12,16] does not in patients with cerebellar damage. More direct evidence showed that plasticity of synaptic transmission efficacy in the cerebellum that was modified by concentration of nitric oxide (NO) played a significant role in locomotive adaptation in decerebrate cat [21]. Interestingly, regarding movement specificity, various aspects of limb movement such as direction, velocity, acceleration and force have been demonstrated to be represented in the cerebellum, as shown by discharge rate in single unit recording in the cerebellum [22]. In the present study, since the subjects performed both walking and running under identical belt speed, in which the limb movements do not simply depend on locomotion speed but are demonstrated to differ across the modes [3], it is possible that there were different representation for each locomotive mode.

Along with the cerebellar function, the contribution of the descending neural drive from the supraspinal centers, especially those from the mesencephalic locomotor region (MLR) in the brainstem, provides an additional explanation for the mode-specificity. For example, in decerebrate salamander, electrical microstimulation at a particular site in the MLR resulted in a phase-dependent electromyographic (EMG) burst and conse-

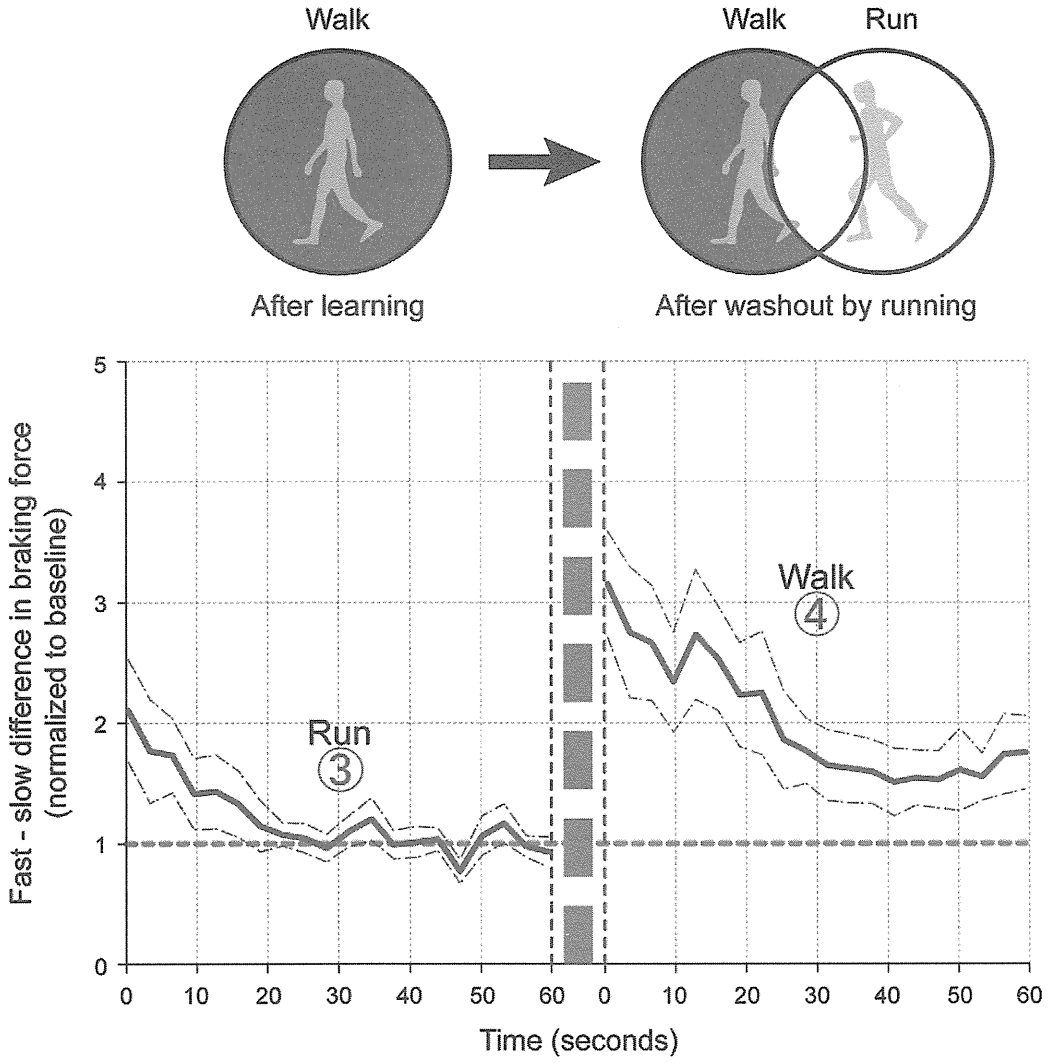

Figure 6. Degree of washout in the stored motor pattern in walking by running (first and second washout periods shown consecutively from Experiment 2). The asymmetrical movement pattern was evident with the initiation of walking (blue lines) despite the symmetrical walking pattern at the end of the first washout period in running (red lines), an indication of only partial washout (also described in the schematic figure). Data are presented as means (thick lines) and their standard errors of the mean (dotted lines).
doi:10.1371/journal.pone.0046349.g006

quently locomotor-like movements of the body [23]. In the emergence of these behaviors, two different locomotor modes (stepping and swimming) were exhibited with different current intensities [23]. Or, more classically, an increase in stimulus intensity to the mid-brain in decerebrate cats walking on a treadmill caused them to gallop [24]. From these results, the intensities in the descending drive may significantly affect the decision of different locomotive modes. In the current study, although speculative, the gait pattern upon the initiation of walking after adapting to run was reactively disturbed (the prominent asymmetry in the first few seconds, shown by the light blue line in Figure 4). This reaction may reflect the component of running. That is, to accelerate the center of body mass upon acceleration of the treadmill by increasing the descending drive from the locomotor centers. Consequently, this could result in the partial emergence of the asymmetrical movement pattern previously acquired in running.

Regarding the specificity in the locomotor center in the spinal cord, on the other hand, it was recently demonstrated that specific sets of spinal interneurons are activated depending on locomotion (swimming) frequency in larval zebrafish [14]. Locomotion behavior in larval zebrafish was previously characterized as having two different modes [25]. One is the mode used to move routinely in water with lower movement frequencies and small yaw amplitudes, while the other is the escape movement with higher frequencies with larger yaws [25]. On the execution of these locomotor behaviors by zebrafish, McLean et al. (2008) [14] showed that, in contrast to motoneurons that are additionally recruited with increasing swimming frequencies following classic size principle, the activities in some sets of interneurons evident

under lower swimming frequency were inhibited during swimming at higher frequencies [14]. In other animal models, such as in a fictive scratching movement in the turtle hindlimb, it was found that different populations of propriospinal neurons were identified with respect to two different modes of scratching movements [13]. Based on these previous results in animal models, it is speculated that the specific structures to be selected in the spinal cord depending on the modes might explain the underlying differences in the neural mechanisms between walking and running in humans.

Regarding adaptation as observed in the present study and in previous studies [11 12,16], the spinal cord itself is known to be capable of adapting locomotor patterns, as predominantly demonstrated in the stepping movement of human infants [26] or in cats that underwent complete spinal cord transection [27]. The relationship between mode specificity and adaptation remains unclear. It is however, reasonable to consider that the acquisition of the novel movement patterns took place in particular sites in the spinal cord or in combination with the higher structures depending on the mode, at least before motoneuron, which is the final common pathway to muscles. The acquired movement patterns were therefore only partially transferred to the opposite modes, which have different responsible sites and were rarely washed out by the execution of the opposite ones.

In summary, the two major modes of human locomotion, walking and running, are not only functions of different speed but have fundamentally different neural control mechanisms. The present results provide extremely important implications for the construction of training regimens in locomotive movements in both athletic training and rehabilitation processes. Further considerations should be made among other locomotive tasks or those under different physical constraints.

Acknowledgments

The authors thank Dr. Bimal Lakhani for editing the English in the manuscript.

Author Contributions

Conceived and designed the experiments: T. Ogawa NK T. Ogata KN. Performed the experiments: T. Ogawa. Analyzed the data: T. Ogawa. Contributed reagents/materials/analysis tools: T. Ogawa NK. Wrote the paper: T. Ogawa NK T. Ogata KN.

References

1. Farley CT, McMahon TA (1992) Energetics of walking and running: insights from simulated reduced-gravity experiments. J Appl Physiol 73: 2709–2712.
2. Prilutsky BI, Gregor RJ (2001) Swing- and support-related muscle actions differently trigger human walk-run and run walk transitions. J Exp Biol 204: 2277–2287.
3. Ivanenko YP, Cappellini G, Dominici N, Poppele RE, Lacquaniti F (2007) Modular control of limb movements during human locomotion. J Neurosci 27: 11149–11161.
4. Sasaki K, Neptune RR (2006) Differences in muscle function during walking and running at the same speed. J Biomech 39: 2005–2013.
5. Cappellini G, Ivanenko YP, Poppele RE, Lacquaniti F (2006) Motor patterns in human walking and running. J Neurophysiol 95: 3426–3437.
6. Diedrich FJ, Warren WH Jr (1995) Why change gaits? Dynamics of the walk-run transition. J Exp Psychol 21: 183–202.
7. Kram R, Domingo A, Ferris DP (1997) Effect of reduced gravity on the preferred walk-run transition speed. J Exp Biol 200: 821–826.
8. Bartlett JL, Kram R (2008) Changing the demand on specific muscle groups affects the walk-run transition speed. J Exp Biol 211: 1281–1288.
9. Nozaki D, Kurtzer I, Scott SH (2006) Limited transfer of learning between unimanual and bimanual skills within the same limb. Nat Neurosci 9: 1364–1366.
10. Ikegami T, Hirashima M, Taga G, Nozaki D (2010) Asymmetric transfer of visuomotor learning between discrete and rhythmic movements. J Neurosci 30: 4515–4521.
11. Choi JT, Bastian AJ (2007) Adaptation reveals independent control networks for human walking. Nat Neurosci 10: 1055–1062.
12. Vasudevan EV, Bastian AJ (2010) Split-belt treadmill adaptation shows different functional networks for fast and slow human walking. J Neurophysiol 103(1): 183–191.
13. Berkowitz A, Stein PSG (1994) Activity of descending propriospinal axons in the turtle hindlimb enlargement during two forms of fictive scratching: phase analysis. J Neurosci 14: 5105–5119.
14. McLean DL, Masino MA, Koh IYY, Lindquist WB, Fetcho JR (2008) Continuous shifts in the active set of spinal interneurons during changes in locomotor speed. Nat Neurosci 11: 1419–1429.
15. Ogawa T, Kawashima N, Nakazawa K, Ogata T (2011) Limited transfer of novel movement pattern between walking and running under same velocity. Soc Neurosci Abstract.
16. Reisman DS, Block HJ, Bastian AJ (2005) Interlimb coordination during locomotion: what can be adapted and stored? J Neurophysiol 94: 2403–2415.
17. Morton SM, Bastian AJ (2006) Cerebellar contributions to locomotor adaptations during splitbelt treadmill walking. J Neurosci 26: 9107–9116.
18. Ito S, Yuasa H, Luo ZW, Ito M, Yanagihara D (1998) A mathematical model of adaptive behavior in quadruped locomotion. Biol Cybern 78: 337–347.
19. Shadmehr R, Mussa-Ivaldi FA (1994) Adaptive representation of dynamics during learning of a motor task. J Neurosci. 14: 3208–3224.
20. Bastian AJ (2006) Learning to predict the future: the cerebellum adapts feedforward movement control. Curr Opin Neurobiol 16: 645–649.
21. Yanagihara D, Kondo I (1996) Nitric oxide plays a key role in adaptive control of locomotion in cat. Proc Natl Acad Sci U S A. 93: 13292–7.
22. Thach WT (1978) Correlation of neural discharge with pattern and force of muscular activity, joint position, and direction of intended next movement in motor cortex and cerebellum. J Neurophysiol 41: 654–676.
23. Cabelguen JM, Bourcier-Lucas C, Dubuc R (2003) Bimodal locomotion elicited by electrical stimulation of the midbrain in the salamander notophathalmus viridescens. J Neurosci 23: 2434–2439.
24. Shik ML, Severin FV, Orlovsky GN (1966) Control of walking and running by means of electrical stimulation of the mid-brain. Biophys 11: 756–765.
25. Budick SA, O'Malley DM (2000) Locomotor repertoire of the larval zebrafish: swimming, turning and prey capture. J Exp Biol 203: 2565–2579.
26. Lam T, Wolstenholme C, Yang JF (2003) How do infants adapt to loading of the limb during the swing phase of stepping? J Neurophysiol 89: 1920–1928.
27. Hodgson JA, Roy RR, De Leon R, Dobkin B, Edgerton VR (1994) Can the mammalian spinal cord learn a motor task? Med Sci Sports Exerc 26: 1491–1497.

NEUROSCIENCE

Phosphorylation of Cytohesin-1 by Fyn Is Required for Initiation of Myelination and the Extent of Myelination During Development

Junji Yamauchi,[1,2,3,4]* Yuki Miyamoto,[1] Tomohiro Torii,[1] Shou Takashima,[1] Kazumi Kondo,[5] Katsumasa Kawahara,[3] Noriko Nemoto,[6] Jonah R. Chan,[7] Gozoh Tsujimoto,[8] Akito Tanoue[1]

Schwann cells respond to cues from axons by transforming their cellular morphology and forming myelin. We demonstrated that the guanine nucleotide exchange factor (GEF) cytohesin-1 promoted myelination by activating the small guanosine triphosphatase (GTPase) Arf6. In mice, ablating *cytohesin-1* delayed myelination and diminished the amount of myelin produced. We determined that the Src-family kinase Fyn phosphorylated tyrosine 382 (Y^{382}) of cytohesin-1, and we generated transgenic mice that expressed a Schwann cell–specific phosphorylation mutant of cytohesin-1 (Y382F) that could not be targeted by Fyn. During development, these transgenic mice displayed delayed myelination compared to that of wild-type mice, as well as a decrease in the amount of myelin produced, similar to that observed in *cytohesin-1*$^{-/-}$ mice. These findings demonstrate that phosphorylation of cytohesin-1 by Fyn is required for full myelination and suggest that tyrosine phosphorylation of GEFs may be a mechanism to activate small GTPases engaged in cell morphogenesis.

INTRODUCTION

During development in the peripheral nervous system, such as in sensory neurons, Schwann cells wrap their plasma membranes concentrically around axons to form a unique multilamellar structure called myelin. The morphologically differentiated plasma membrane of the Schwann cell acts as an insulator that surrounds axons and markedly enhances the propagation of the action potential along the axon (*1*, *2*). Many growth factors and adhesion molecules found on neuronal axons bind to their cognate receptors on Schwann cells and control the spatial and temporal regulation of myelination (*1*–*4*). Although these intermolecular signals have been extensively studied, little is known about the relevant intracellular signaling mechanisms that specially transduce axonal cues for the morphological changes in Schwann cells that are necessary to initiate myelination and determine the number of wraps of membrane to be deposited (*3*, *4*). For example, although it is well established that the number of concentric wraps of membrane correlates with axon diameter and the relative abundance of the growth factor neuregulin-1 (NRG1) type III (*3*), it is unclear how intracellular signaling pathways respond to modulate the dynamic morphological changes necessary to accomplish this task.

The Rho guanosine triphosphatases (GTPases) Rac1 and Cdc42 promote Schwann cell proliferation and migration, as well as the radial sorting of axons by Schwann cells before the initiation of myelination (*5*–*7*). Additionally, the Cdc42 effector neural Wiskott-Aldrich syndrome protein (N-WASP), a known activator of the Arp2/3 complex, is essential for proper myelination of axons by Schwann cells (*8*, *9*).

In addition to the Rho-family GTPases, evidence indicates that small GTPases of the Arf family also contribute to signal-dependent cell morphological changes in Schwann cells (*10*–*13*). Similarly to Rho GTPases, Arfs act as molecular switches; they are biologically active when bound to guanosine triphosphate (GTP) and inactive when bound to guanosine diphosphate (GDP) (*10*, *11*). Two types of regulatory proteins, guanine nucleotide exchange factors (GEFs) and GTPase-activating proteins (GAPs), control the guanine nucleotide–binding states of the GTPases. GEFs catalyze the exchange reaction of GDP with GTP to generate active GTPases. This reaction is a very important rate-limiting step because GEFs determine the activation of specific GTPases by integrating upstream signals in cells (*12*, *13*). Cytohesin-1 [also known as the B2-1 clone or pleckstrin homology (PH), Sec7, and coiled-coil domains 1 (PSCD1)] is such a protein, which controls GDP-GTP exchange reactions (*14*–*18*). Cytohesin-1, which is now known as one of the four members of the cytohesin family of GEFs for Arf1 and Arf6, was identified as a binding partner of the intracellular region of lymphocyte β_2 integrins (*16*, *17*). Here, we describe how signaling through cytohesin-1 mediated myelination of axons by Schwann cells. In addition, we found that the tyrosine kinase Fyn was a binding partner of cytohesin-1 in Schwann cells and that it acted upstream of cytohesin-1 by phosphorylating tyrosine 382 (Y^{382}). Fyn belongs to the Src family of tyrosine kinases, members of which couple extracellular signals to transducing intracellular ones (*19*). Our experiments also present evidence suggesting that the direct tyrosine phosphorylation of GEFs might be a general mechanism for the activation of small GTPases involved in cell morphological changes.

RESULTS

Cytohesin-1 is necessary for myelination by Schwann cells

To thoroughly examine a role for small GTPase function in the initiation and formation of myelin by Schwann cells, we initiated studies with various small-molecule inhibitors of proteins involved in GTPase signaling pathways. In experiments with cocultures of purified Schwann cells and dorsal root ganglion (DRG) neurons (*20*), we found that SecinH3 markedly inhibited myelination of DRG neurons by ~75% compared to that in control cocultures (Fig. 1, A and B). SecinH3 is a chemical compound that

[1]Department of Pharmacology, National Research Institute for Child Health and Development, Setagaya, Tokyo 157-8535, Japan. [2]Department of Biological Sciences, Tokyo Institute of Technology, Midori, Yokohama 226-8501, Japan. [3]Department of Physiology, Kitasato University School of Medicine, Sagamihara, Kanagawa 252-0374, Japan. [4]The Japan Human Health Sciences Foundation, Chuo, Tokyo 103-0001, Japan. [5]Otsuka Pharmaceutical Co. Ltd., Kawauchi, Tokushima 771-0192, Japan. [6]Bioimaging Research Center, Kitasato University School of Medicine, Sagamihara, Kanagawa 252-0374, Japan. [7]Department of Neurology, University of California, San Francisco, San Francisco, CA 94158, USA. [8]Department of Pharmacogenomics, Graduate School of Pharmaceutical Sciences, Kyoto University, Sakyo, Kyoto 606-8501, Japan.
*To whom correspondence should be addressed. E-mail: jyamauchi@nch.go.jp

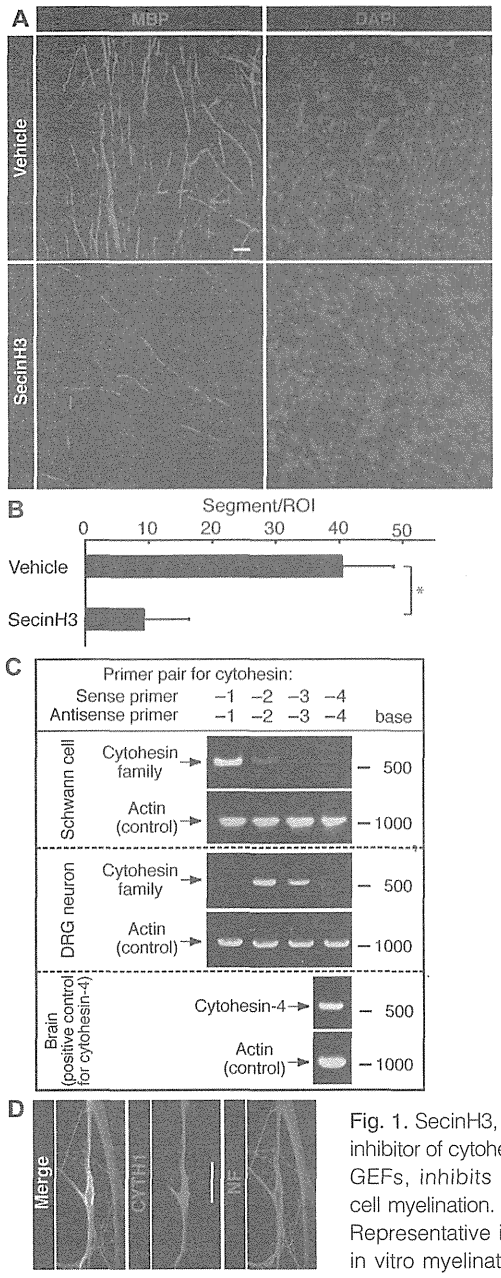

Fig. 1. SecinH3, a specific inhibitor of cytohesin-family GEFs, inhibits Schwann cell myelination. (A and B) Representative images of in vitro myelination in co-cultures of rat Schwann cells and DRG neurons in the presence or absence of 10 μM SecinH3. Co-cultures were incubated with an anti-MBP antibody to stain myelin (red) and with 4′,6-diamidino-2-phenylindole (DAPI) to stain nuclei (blue). Scale bar, 20 μm. The myelin segments in a 200-μm^2 field were counted. Data are presented as the numbers of myelin segments per region of interest (ROI) and were evaluated by one-way analysis of variance (ANOVA). *$P < 0.01$; $n = 5$ experiments. (C) RT-PCR analysis of members of the cytohesin family of GEFs, and of actin as a control, in rat Schwann cells, DRG neurons, and brain. Data are representative of three experiments. (D) Cocultures of rat Schwann cells and DRG neurons were costained with antibodies against cytohesin-1 (green) and neurofilament (NF, red). Scale bar, 25 μm. Cytohesin-1 was primarily expressed in Schwann cells. Data are representative of three experiments.

specifically inhibits all members of the cytohesin family of GEFs (which includes cytohesin-1, -2, -3, and -4) but does not inhibit other types of Arf GEFs (*21*, *22*). We estimated the extent of myelination by visualizing myelin segments with an antibody against myelin basic protein (MBP). We thus sought to confirm the presence of cytohesin family members in Schwann cells. Reverse transcription polymerase chain reaction (RT-PCR) analysis primarily detected cytohesin-1, which was found in Schwann cells but not in neurons (Fig. 1C). Immunofluorescence analysis of cocultures enabled us to detect cytohesin-1 protein in Schwann cells (Fig. 1D and fig. S1A). Immunohistochemical analysis of longitudinal sections of sciatic nerves confirmed the localization of cytohesin-1 in Schwann cells (fig. S1B). An affinity-purified antibody against cytohesin-1 was used in staining (fig. S2, A and B). In addition, affinity precipitation assays with Golgi-associated, γ-adaptin ear–containing, Arf-binding protein 3 (GGA3), which specifically binds to the active, GTP-bound forms of Arf1 and Arf6 (*21*, *22*), illustrated that Arf6 in Schwann cells was indeed specifically activated by cytohesin-1 after stimulation of Schwann cells with neuronal conditioned medium (CM) because Arf6 activation was blocked by knockdown of cytohesin-1 (Fig. 2, A and B). In contrast, Arf1 activation was not dependent on cytohesin-1. Stimulation with neuronal CM did not result in detectable changes in the amounts of *cytohesin-1*, *-2*, *-3*, or *-4* mRNAs (fig. S3). Given that Arf6 and the Rho GTPases are critical for dynamic cell morphological changes (*10*–*13*), these results suggest

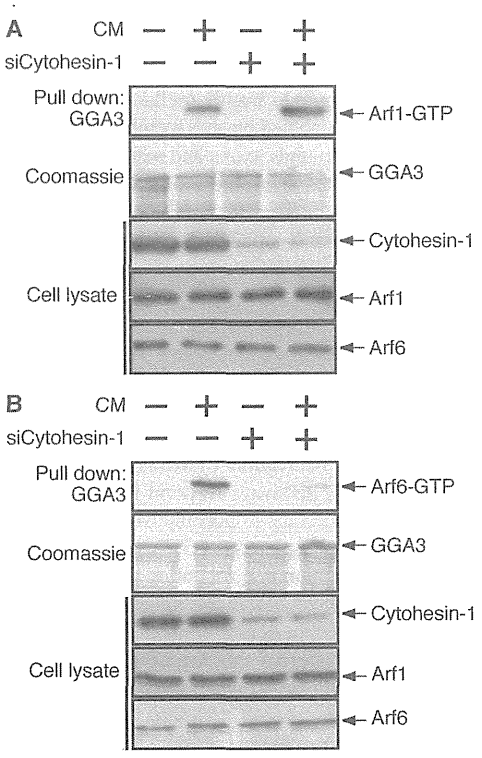

Fig. 2. Cytohesin-1 acts as a GEF for Arf6, but not Arf1, in Schwann cells. (A and B) Rat Schwann cells were transfected with control siRNA or cytohesin-1–specific siRNA (siCytohesin-1). Forty-eight hours after transfection, cells were left unstimulated or were stimulated with neuronal CM for 30 min. Cells were then lysed and used for affinity precipitation with GST-GGA3 to pull down and detect active (A) GTP-bound Arf1 and (B) GTP-bound Arf6 by Western blotting. Western blotting analysis for total cytohesin-1 and Arf proteins and Coomassie staining of GGA3 were also performed. Data are representative of three experiments.

that cytohesin-1 and Arf6 may contribute to Schwann cell development and myelination.

Fyn directly activates cytohesin-1 by phosphorylating Tyr^{382}

To investigate how cytohesin-1 was regulated in Schwann cells, we expressed the myc-tagged PH domain of cytohesin-1 in the immortalized Schwann cell line RT4-D6P2T and collected PH domain–interacting proteins with a resin conjugated to an antibody against myc (Fig. 3A). Cytohesin-family GEFs commonly consist of three domain structures: the N-terminal region containing the coiled-coil (CC) structure, the catalytic Sec7 domain, and the C-terminal region containing the PH domain, which provides a platform for binding to various signaling molecules in a range of different cell types (*12*, *13*, *23*, *24*). Through silver staining and mass spectrometric (MS) analysis of electrophoretically separated proteins, we identified the Src-family tyrosine kinase Fyn as the ~60-kD protein that interacted with the PH domain of cytohesin-1 (Fig. 3B). Previous findings suggested that Fyn promotes myelination by Schwann cells in coculture (*25*) and myelination by oligodendrocytes in vivo (*26*). RT-PCR analysis showed that Fyn mRNA was more abundant in Schwann cells than were those of other members of the Src family (Fig. 3C), and autophosphorylation of Fyn was detected in Schwann cells after stimulation with CM (Fig. 3D). Reciprocally, stimulation of Schwann cells with CM decreased the phosphorylation state of Fyn at Tyr^{531} (Fig. 3E), which is an inhibitory phosphorylation site (*19*). Tyr^{531} of Fyn corresponds to Tyr^{527} of Src. In addition, CM increased the affinity-precipitated active form of cytohesin-1, whereas knockdown of Fyn blocked the association with guanine nucleotide–free Arf6 (Fig. 3F). The affinity precipitation assay is based on the property that catalytically active GEFs preferentially interact with guanine nucleotide–free GTPases (fig. S4) (*7*, *27*–*29*). We observed similar effects in the case of Arf6 activation (Fig. 3F), demonstrating that Fyn regulates cytohesin-1 and Arf6 as a specific signaling complex.

To analyze the interaction of Fyn with cytohesin-1, we transfected human embryonic kidney (HEK) 293T cells with plasmid encoding wild-type cytohesin-1, which we then purified (fig. S5A) and showed to be free of either Arf1 or Arf6 (fig. S5B). We demonstrated that recombinant Fyn tyrosine-phosphorylated wild-type cytohesin-1 and that Fyn and cytohesin-1 were coimmunoprecipitated in vitro (Fig. 4A). Fyn bound

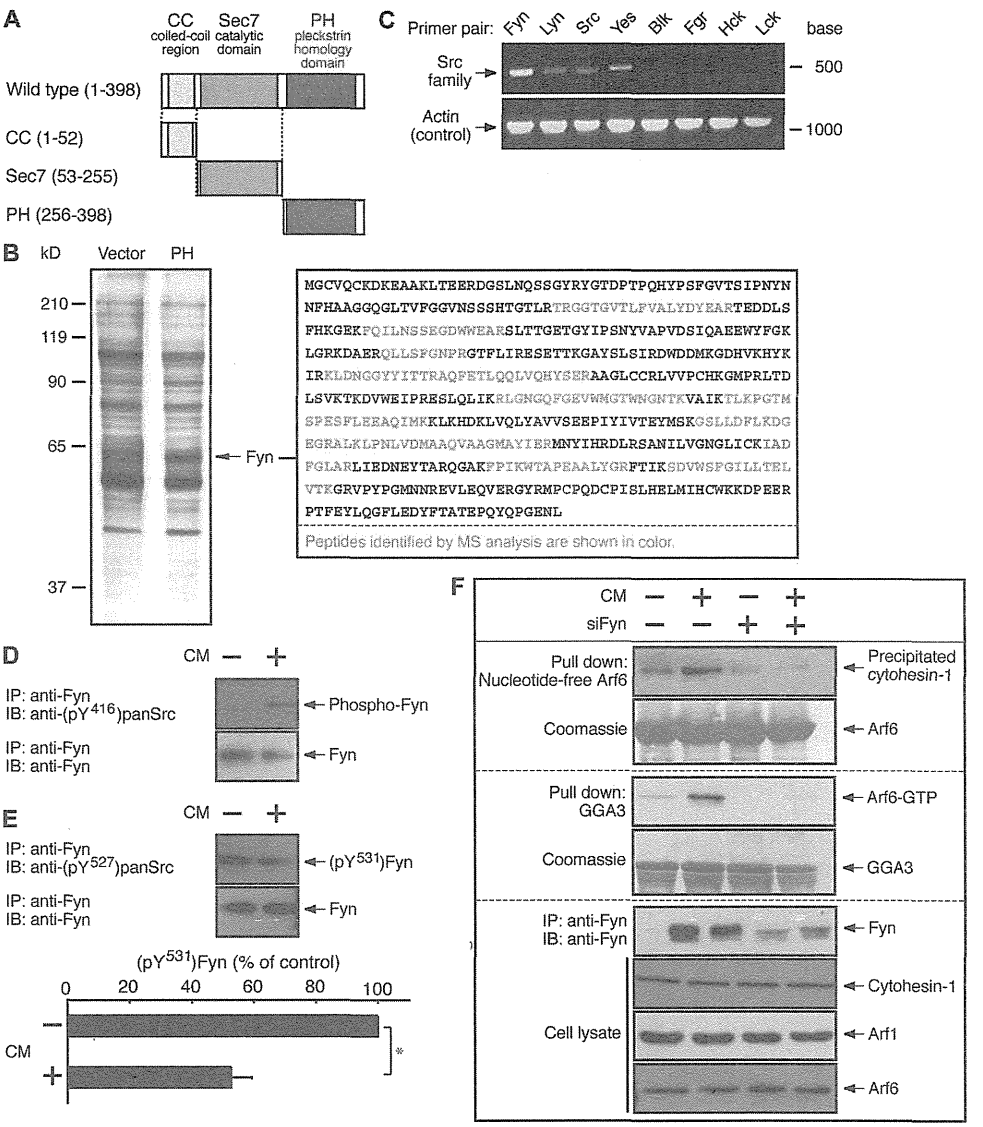

Fig. 3. Fyn mediates activation of cytohesin-1 and Arf6 in Schwann cells. (A) Schematic diagram of the domain organization of cytohesin-1 showing the CC, Sec7, and PH domains. (B) RT4-D6P2T cells were transfected with pCMV or pCMV–myc–cytohesin-1–PH, lysed, and incubated with an anti-myc resin. The ~60-kD silver-stained protein band indicates specific binding to the PH domain as shown on the left and was identified through MS analysis as Fyn. Fyn peptides identified by MS analysis are shown in color on the right. (C) RT-PCR analysis of the Src family members in rat Schwann cells. Data are representative of three experiments. (D) Schwann cells were left unstimulated or were stimulated with CM, lysed, and subjected to immunoprecipitation (IP) with an anti-Fyn antibody. The immunoprecipitated samples were analyzed by Western blotting (IB) with an anti-(pY^{416})panSrc antibody, which recognizes active (phosphorylated at Tyr^{416}) Src family members, or with an anti-Fyn antibody. Data are representative of three experiments. (E) Top: The same immunoprecipitated samples were also analyzed by Western blotting with an anti-(pY^{527})panSrc antibody, which recognizes an inhibitory phosphorylation site of the Src family members (which corresponds to Tyr^{531} in Fyn), or with an anti-Fyn antibody. Bottom: Bar chart quantifying the band intensities of (p531Y)Fyn. Data were evaluated by one-way ANOVA. *$P < 0.01$; $n = 3$ experiments. (F) Schwann cells were transfected with control siRNA or Fyn-specific siRNA (siFyn) and were left untreated or were treated with CM. Cell lysates were then subjected to affinity precipitation with GST-tagged GGA3 or guanine nucleotide–free Arf6, and Western blotting analysis was performed to detect total Fyn, cytohesin-1, and the Arf proteins. Data are representative of three experiments.

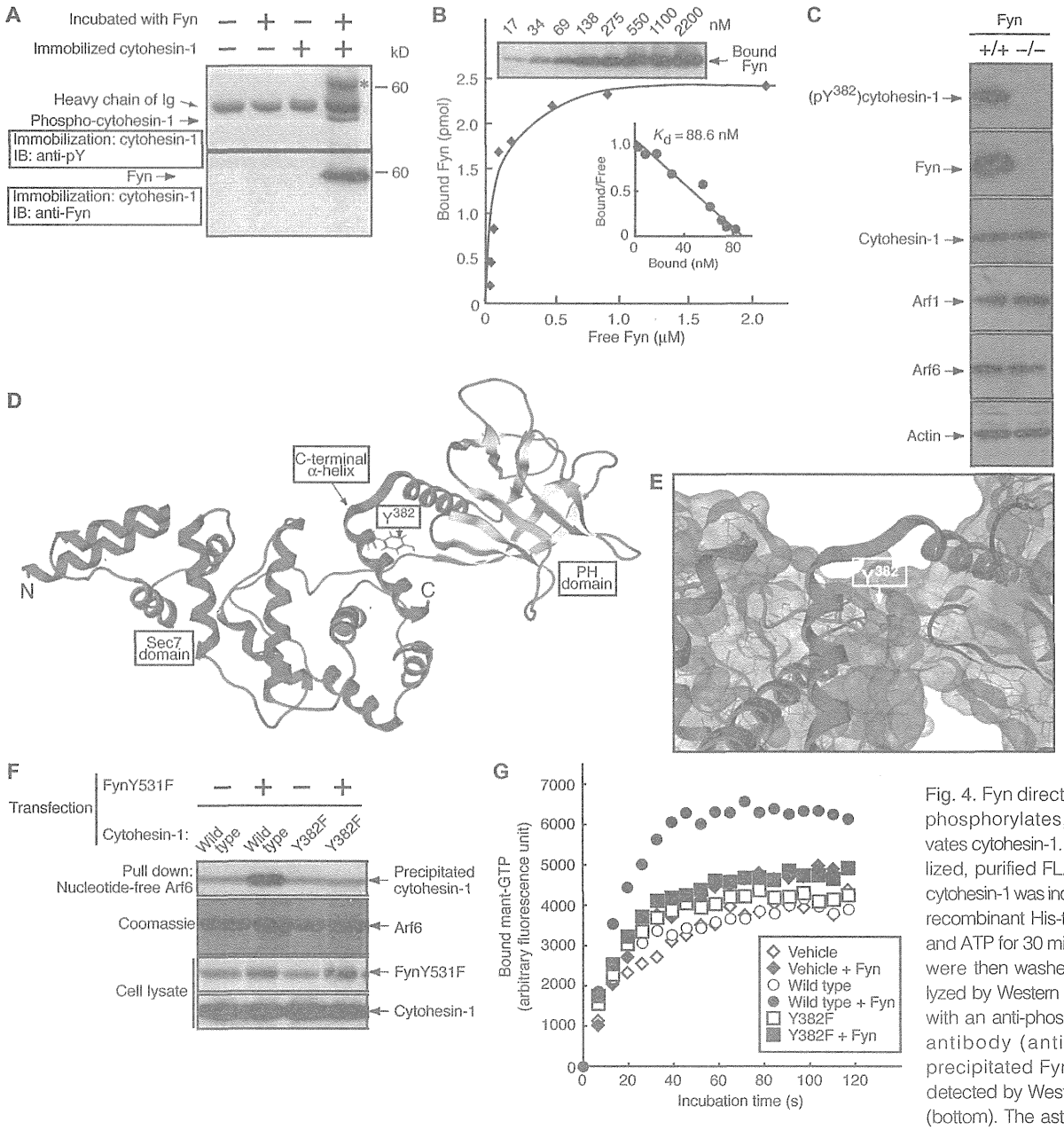

Fig. 4. Fyn directly binds to, phosphorylates, and activates cytohesin-1. (A) Immobilized, purified FLAG-tagged cytohesin-1 was incubated with recombinant His-tagged Fyn and ATP for 30 min. Samples were then washed and analyzed by Western blotting (IB) with an anti-phosphotyrosine antibody (anti-pY). Coprecipitated Fyn was also detected by Western blotting (bottom). The asterisk corresponds to the position of autophosphorylated Fyn. Data are representative of three experiments. (B) Quantitative analysis of the interaction between FLAG–cytohesin-1 and His-Fyn was performed. His-Fyn protein (17 to 2200 nM) was mixed with immobilized FLAG–cytohesin-1 (30 μg) for 2 hours. The resin was washed, subjected to SDS–polyacrylamide gel electrophoresis (SDS-PAGE), and analyzed by Western blotting with an anti-His antibody for bound His-Fyn. Scatchard analysis revealed a K_d value of 88.6 nM. Data are representative of three experiments. (C) Immunoprecipitates with an anti–cytohesin-1 antibody using samples of 7-day-old sciatic nerve extracts of Fyn-knockout mice (−/−) and littermate controls (+/+) were subjected to immunoprecipitation with an antibody against cytohesin-1 and were analyzed by Western blotting with an anti-(pY^{382}) cytohesin-1 antibody as well as with antibodies against the indicated proteins. Data are representative of three experiments. (D) Generated model of mouse cytohesin-1 (amino acid residues 60 to 394) based on the three-dimensional (3D) structure of human cytohesin-3. The Sec7 domain and the helical region in the C-terminal position are indicated in red, whereas the β sheet structure of the PH domain is indicated in yellow. Y^{382} of cytohesin-1 in the C-terminal helical region is predicted to be positioned above the catalytic Sec7 domain. (E) Molecular modeling of the interactive structure between the catalytic Sec7 domain (green background) and the C-terminal helical region (red helix). (F) HEK 293T cells were cotransfected with plasmid encoding the constitutively active mutant FynY531F and with plasmid encoding either FLAG–cytohesin-1 or FLAG–cytohesin-1Y382F. Forty-eight hours after transfection, cells were lysed and subjected to affinity precipitation with GST-tagged, guanine nucleotide–free Arf6. The abundances of the Fyn and cytohesin-1 constructs and of precipitated GST-Arf6 are shown. Data are representative of three experiments. (G) His-Fyn tyrosine phosphorylation reaction of FLAG–cytohesin-1 or the Y382F mutant protein was performed and their guanine nucleotide–binding reactions for His-Arf6 by phosphorylated cytohesin-1 protein were measured. Data show the amount of fluorescent mant-GTP bound to His-Arf6. Data are representative of three experiments.

to cytohesin-1 with a dissociation constant (K_d) of 88.6 nM (Fig. 4B), indicating probable direct binding.

To determine the specific phosphorylation site of cytohesin-1, we generated constructs encoding each of the domains of cytohesin-1. Fyn specifically phosphorylated the PH domain in tandem with the predicted helical region, and as expected, Fyn coimmunoprecipitated with the cytohesin-1 PH domain (fig. S6A). Reciprocally, cytohesin-1 specifically interacted with the Src homology 1 (SH1) domain (which contains the kinase domain) of Fyn (fig. S7, A and B), demonstrating that binding occurred between the PH domain of cytohesin-1 and the kinase domain of Fyn. We next constructed phosphorylation mutants of cytohesin-1 harboring a tyrosine to phenylalanine (Y382F) mutation in the PH domain (fig. S6B) and assessed the extent of its phosphorylation by Fyn. We identified Tyr^{382} as a specific phosphorylation site for Fyn (fig. S6C) and found that the Y382F mutation in cytohesin-1 completely abolished phosphorylation by Fyn (fig. S6D). In addition, in sciatic nerves from Fyn-knockout mice, phosphorylation of cytohesin-1 at Tyr^{382} was undetectable (Fig. 4C and fig. S8, A and B), indicating that Fyn phosphorylated Tyr^{382} in vivo.

Amino acid alignment analysis of cytohesin-family GEFs illustrated conservation of Tyr^{382} (fig. S9, A and B). Tyr^{382} is found within the C-terminal, autoinhibitory helical region in the predicted steric model (Fig. 4, D and E), implying the particular importance of Tyr^{382} for the regulation of cytohesin-1. This model was based on cytohesin-3 (*30*). Indeed, when coexpressed with active Fyn harboring a mutation in its inhibitory phosphorylation site, wild-type cytohesin-1, but not the Y382F mutant, was affinity-precipitated with guanine nucleotide–free Arf6 (Fig. 4F). To assay the guanine nucleotide

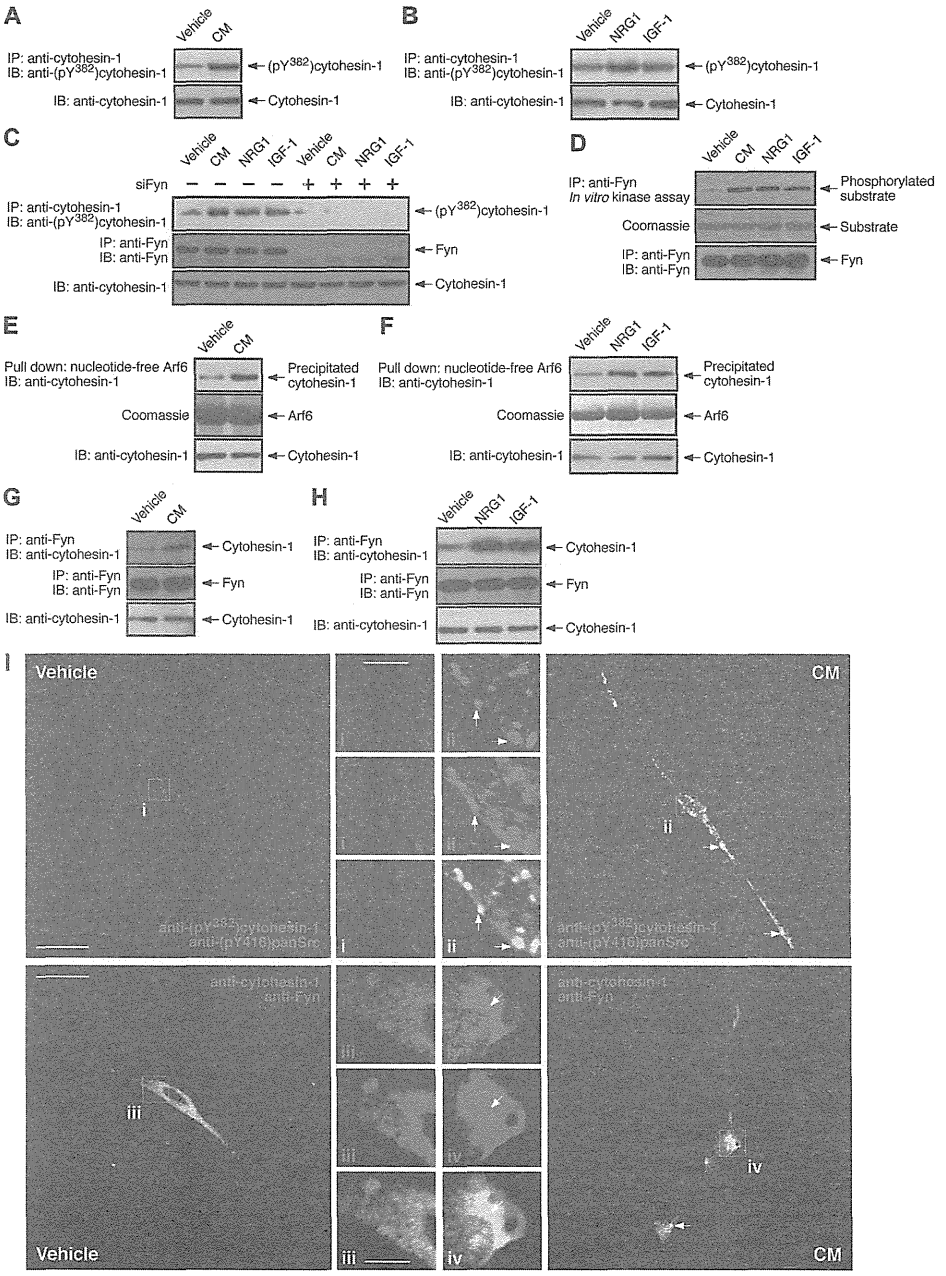

Fig. 5. In Schwann cells, Fyn forms a complex with cytohesin-1, phosphorylates it at Tyr^{382}, and activates it. (A and B) Rat Schwann cells were incubated with CM or a growth factor (NRG1 or IGF-1) for 30 min. Cells were then lysed and subjected to immunoprecipitation (IP) with an anti–cytohesin-1 antibody and analyzed by Western blotting (IB) with an anti–(pY382)cytohesin-1 antibody and an antibody against total cytohesin-1 protein. (C) Rat Schwann cells, which were transfected with control or Fyn-specific siRNA, were incubated with CM or a growth factor (NRG1 or IGF-1). Cell lysates were subjected to immunoprecipitation with an anti–cytohesin-1 antibody and Western blotting analysis with an anti–(pY382)cytohesin-1 antibody. The abundances of Fyn and total cytohesin-1 were also determined. (D) In vitro kinase assays were performed with immunoprecipitated Fyn with the GST-PH domain as the substrate. (E and F) After stimulation of cells with CM or a growth factor (NRG1 or IGF-1) for 30 min, affinity precipitation with GST-tagged, guanine nucleotide–free Arf6 was performed. Total cytohesin-1 and GST-Arf6 were also examined. (G and H) After stimulation with CM or a growth factor (NRG1 or IGF-1) for 30 min, cells were lysed and subjected to immunoprecipitation with an anti-Fyn antibody and then analyzed by Western blotting with an antibody against cytohesin-1 or Fyn. Total cytohesin-1 was also determined. (I) Top: Immunofluorescence images of (pY382)cytohesin-1 (green) with (pY416)panSrc (red) in cells after stimulation with or without CM. Bottom: Immunofluorescence images of cytohesin-1 (green) with Fyn (red). Insets [(i) to (iv); scale bar, 10 μm] are magnifications of the boxed areas [(i) to (iv)] in the images (scale bar, 25 μm). Arrows indicate representative colocalization regions. All data are representative of three experiments.

exchange reaction, we purified the Y382F mutant protein (fig. S10, A and B) and Arf6 proteins (fig. S10C). When the wild-type or Y382F mutant cytohesin-1 protein was incubated with recombinant Fyn in an experiment to quantify the guanine nucleotide–binding kinetics of Arf6, we found that wild-type cytohesin-1 promoted the binding of cytohesin-1 to Arf6, whereas the Y382F mutant cytohesin-1 abolished it (Fig. 4G), consistent with the results of the guanine nucleotide–releasing assay (fig. S10D). These findings demonstrated that Fyn activated cytohesin-1 by phosphorylating it.

Therefore, we confirmed that cytohesin-1 was phosphorylated in Schwann cells and that CM from neurons enhanced Tyr^{382} phosphorylation (Fig. 5A). In addition, NRG1 and insulin-like growth factor 1 (IGF-1), which are contained in CM and are known to promote myelination by Schwann cells (*2*, *3*, *7*), stimulated phosphorylation of cytohesin-1 (Fig. 5B). Because the effect of IGF-1 alone was very weak but the effect of NRG1 alone was not, it is possible that growth factors in the CM cooperatively led to the phosphorylation of cytohesin-1. We found that phosphorylation of cytohesin-1 was blocked by knockdown of Fyn (Fig. 5C), whose kinase activity was stimulated by CM, NRG1, and IGF-1 (Fig. 5D), indicating that Fyn mediated the Tyr^{382} phosphorylation of cytohesin-1 in Schwann cells. Consistent with these data, CM and the respective growth factors enhanced the amount of active cytohesin-1 (Fig. 5, E and F), and cytohesin-1 was coimmunoprecipitated with Fyn (Fig. 5, G and H). The addition of CM also enhanced the colocalization of Fyn and cytohesin-1 in the cytoplasmic region of Schwann cells (Fig. 5I), findings that were consistent with the biochemical data.

Cytohesin-1 is required for myelination by Schwann cells

To investigate whether cytohesin-1 was involved in the regulation of myelination by Schwann cells and whether Tyr^{382} phosphorylation of cytohesin-1 affected myelination, we performed Western blotting analysis to monitor the abundance of cytohesin-1 and the extent of its phosphorylation at Tyr^{382} during sciatic nerve development. We found that the abundance of cytohesin-1 protein gradually increased from late embryonic stages to postnatal day 14 and then decreased in adulthood. On the other hand, the extent of Tyr^{382} phosphorylation of cytohesin-1 remained increased from late embryonic periods to early postnatal stages

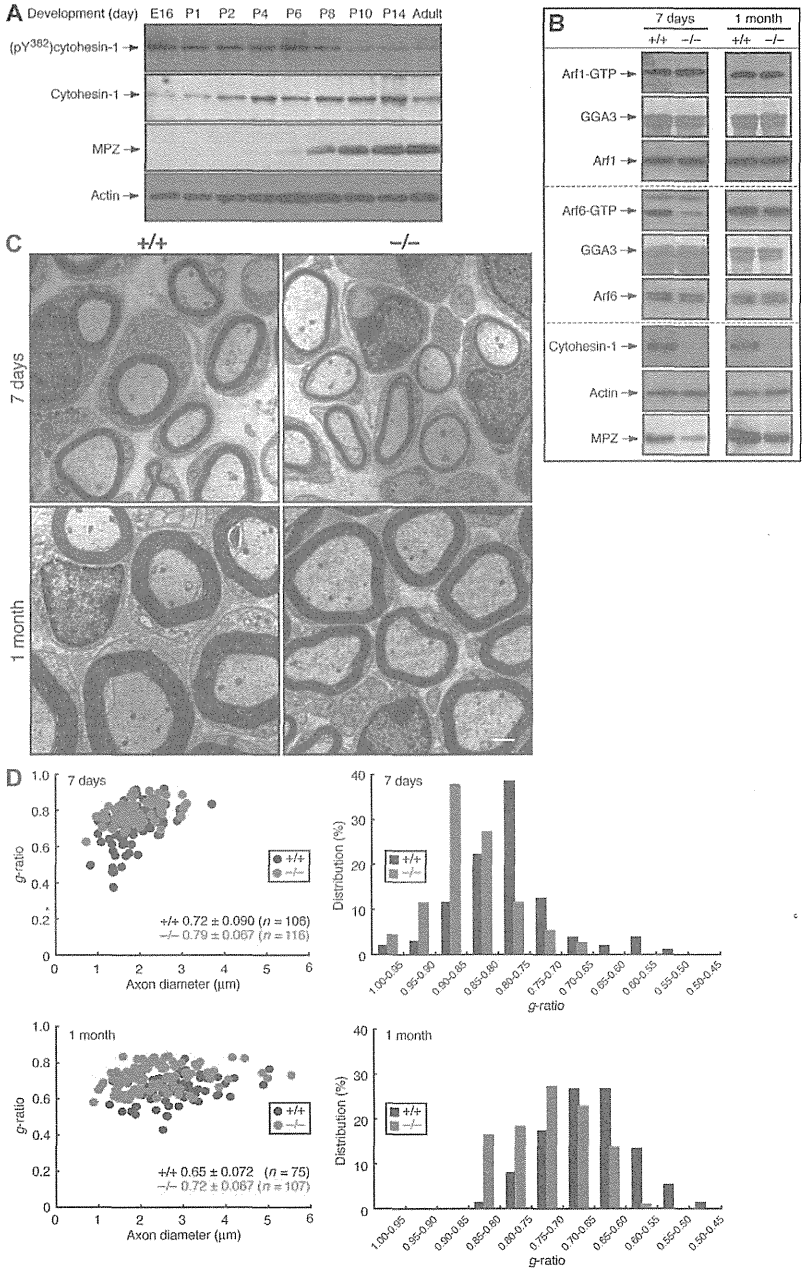

Fig. 6. *Cytohesin-1*$^{-/-}$ mice exhibit decreased myelin thickness in sciatic nerves. (A) The amounts of (pY^{382})cytohesin-1, cytohesin-1, and MPZ in mouse sciatic nerve extracts at embryonic day 16 (E16), at postnatal days 1 to 14 (P1 to P14), and upon adulthood were detected by Western blotting analysis. (B) Affinity precipitation assay of active Arf1 or Arf6 was performed with sciatic nerve extracts from 7-day-old or 1-month-old *cytohesin-1*$^{+/+}$ or *cytohesin-1*$^{-/-}$ mice. The abundances of cytohesin-1, Arf1, Arf6, and MPZ were also determined. Data are representative of three experiments. (C) Representative electron micrographs of five cross-sections of sciatic nerves from 7-day-old or 1-month-old *cytohesin-1*$^{-/-}$ mice (−/−) and wild-type littermate controls (+/+). Scale bar, 1 μm. (D) The *g*-ratio is plotted for each axon size. The average *g*-ratios are shown as scatter plots on the left (n = 116 and 106 experiments for 7-day-old *cytohesin-1*$^{-/-}$ mice and littermate controls, respectively; n = 107 and 75 experiments for 1-month-old *cytohesin-1*$^{-/-}$ mice and littermate controls, respectively). Data are also presented in the form of relative distributions of the *g*-ratios in the bar graphs on the right.

and was diminished upon expression of the myelin marker protein myelin protein zero (MPZ) (Fig. 6A), suggesting a potential role for Tyr^{382} phosphorylation of cytohesin-1 in the initiation of myelination.

We next generated cytohesin-1–knockout (*cytohesin-1*$^{-/-}$) mice (fig. S11, A to C). Deletion of *cytohesin-1* did not detectably alter either the relative amounts of various control proteins (fig. S11D) or the transcription factors Oct6 (also known as Scip or Pou3f1) and Krox20 (also known as Egr2), which control Schwann cell differentiation and development (*2*, *3*) (fig. S12), or the numbers of Schwann cells in the sciatic nerves (fig. S13, A and B). Cross-sectional analysis of sciatic nerves displayed DAPI-positive, nuclei-containing cell bodies of Schwann cells but not neurons. The neurons in the sections contained only axonal processes. On the other hand, decreased levels of Arf6, but not Arf1, activity and MPZ abundance were clearly evident in Western blots when compared to littermate controls at 7 days after birth (Fig. 6B). One month after birth, Arf6 activity and MPZ abundance in *cytohesin-1*$^{-/-}$ mice were similar to those of wild-type littermate controls. Myelination in rodents is initiated after birth and remains active for ~1 month (*1*, *2*). It was thus likely that cytohesin-1 preferentially participated in an early myelination process.

Electron microscopic (EM) analysis illustrated that sciatic nerves from *cytohesin-1*$^{-/-}$ mice exhibited a decrease in myelin extent when compared to sciatic nerves from their wild-type littermate controls (Fig. 6C). These findings were evident from quantification of the average *g*-ratio, which is the numerical ratio between the diameter of the axon and the outer diameter of the myelinated fiber. That is, the smaller the number of the average *g*-ratio, the larger the extent of myelination. At 7 days after birth, the average *g*-ratios in the *cytohesin-1*$^{-/-}$ mice were 0.79 ± 0.067. In contrast, wild-type littermate controls displayed *g*-ratios of 0.72 ± 0.090 (Fig. 6D). The values that we observed in the littermate controls agreed with those reported previously (*31*). At an earlier postnatal stage (3 days), the average *g*-ratios in the *cytohesin-1*$^{-/-}$ mice were 0.87 ± 0.052, whereas wild-type littermate controls displayed *g*-ratios of 0.75 ± 0.066 (fig. S14, A and B). Furthermore, the average *g*-ratios in 1-month-old *cytohesin-1*$^{-/-}$ mice were 0.72 ± 0.067 compared to 0.65 ± 0.072 in littermate controls (Fig. 6, C and D). After 2 months, the average *g*-ratios in *cytohesin-1*$^{-/-}$ mice were 0.73 ± 0.055 compared to 0.68 ± 0.057 in littermate controls (fig. S14, A and B), revealing an overall reduction in myelin extent in the knockout animals. These results are also consistent with those based on Schwann cell–neuronal cultures established from *cytohesin-1*$^{-/-}$ mice. Deletion of *cytohesin-1* decreased myelination by ~70% (Fig. 7, A and B).

Phosphorylation of Tyr^{382} of cytohesin-1 is important in myelination

To determine the role of Tyr^{382} phosphorylation of cytohesin-1 in myelination, we injected a DNA fragment containing the coding sequence of the Y382F mutant of cytohesin-1 with a Moloney murine leukemia virus (MoMLV) intron under the mouse *glial fibrillary acidic protein* (*gfap*) promoter into fertilized mouse oocytes to generate transgenic mice expressing the mutant cytohesin-1 protein. GFAP promoters are active in Schwann cells until the initiation of myelination, after which they then gradually decrease in activity (*32*, *33*). In two of the resulting transgenic mouse lines (TG#1 and TG#5), the Y382F mutant was specifically expressed in Schwann cells but not in neurons. The abundance of the Y382F mutant cytohesin-1 protein was greater in TG#5 Schwann cells than in TG#1 Schwann cells (Fig. 8A), suggesting that protein abundance was dependent on the copy number of the transgene (fig. S15, A to D). We next tested whether the presence of the Y382F mutant in Schwann cells inhibited myelination. We established Schwann cell–neuronal cultures from both transgenic mice. Expression of the Y382F mutant decreased myelination by 70 to 80% and ~90% in the TG#1 and TG#5 cultures, respectively, compared to that in cultures from the control nontransgenic littermates (Fig. 8, B and C), indicating that phosphorylation of Tyr^{382} of cytohesin-1 played an essential role in myelination in vitro.

The relative abundances of various control proteins (Fig. 9A) or of the transcription factors Oct6 and Krox20 (fig. S16) in the sciatic nerves were not detectably altered in the transgenic mice. Immunohistochemical analysis demonstrated that the numbers of Schwann cells in the sciatic nerves of the transgenic mice were similar to those of their wild-type littermate controls (fig. S17, A to D). In contrast, transgenic mice specifically exhibited decreased tyrosine phosphorylation of endogenous cytohesin-1 but not that of the known Fyn substrate p190RhoGAP (*19*, *34*). In addition, the extent of Arf6 activity and the abundance of MPZ were decreased in transgenic mice compared to those of wild-type littermate controls (Fig. 9A).

EM analysis illustrated that sciatic nerves from transgenic mice had decreased myelin thickness compared to those from nontransgenic mice (Fig. 9B). These findings were evident from quantification of the average *g*-ratios. The average *g*-ratios obtained from 8-day-old TG#1 and TG#5 mice were 0.73 ± 0.068 and 0.77 ± 0.063, respectively, whereas the corresponding nontransgenic littermates had average *g*-ratios of 0.69 ± 0.066 and 0.71 ± 0.063 (Fig. 9C). That TG#5 mice displayed more copy numbers and enhanced expression of the transgene than did TG#1 mice positively correlated with the associated decreases in cytohesin-1 phosphorylation, Arf6 activity, MPZ abundance, and myelin thickness. Additionally, the numbers of entirely myelinated axons were 360 ± 44 and 380 ± 32 in 8-day-old TG#1 mice and littermate controls, respectively. Similar results

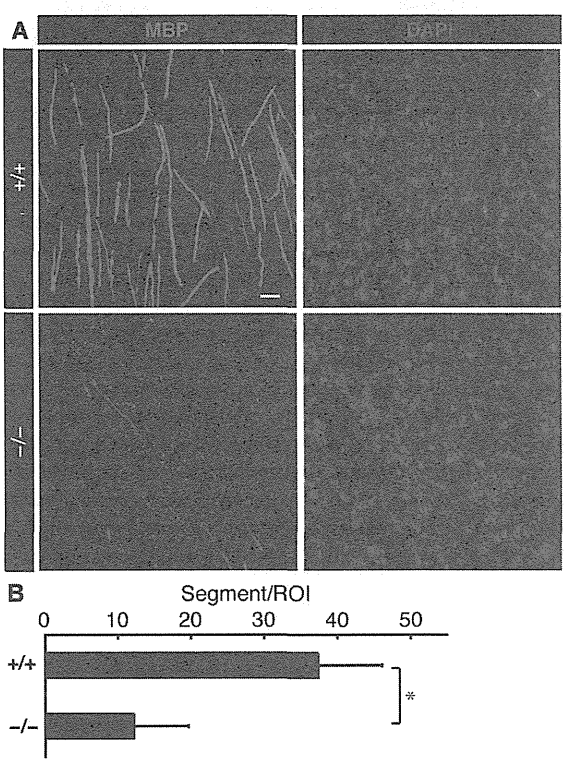

Fig. 7. Deletion of *cytohesin-1* inhibits myelination in vitro. (A) Representative images of in vitro myelination from cultures established from *cytohesin-1*$^{-/-}$ mice (−/−) and littermate controls (+/+). Cultures were stained with an anti-MBP antibody (red) and DAPI (blue). Scale bar, 20 μm. (B) The number of myelin segments was also determined. Data were evaluated by one-way ANOVA (*$P < 0.01$; $n = 5$ experiments).

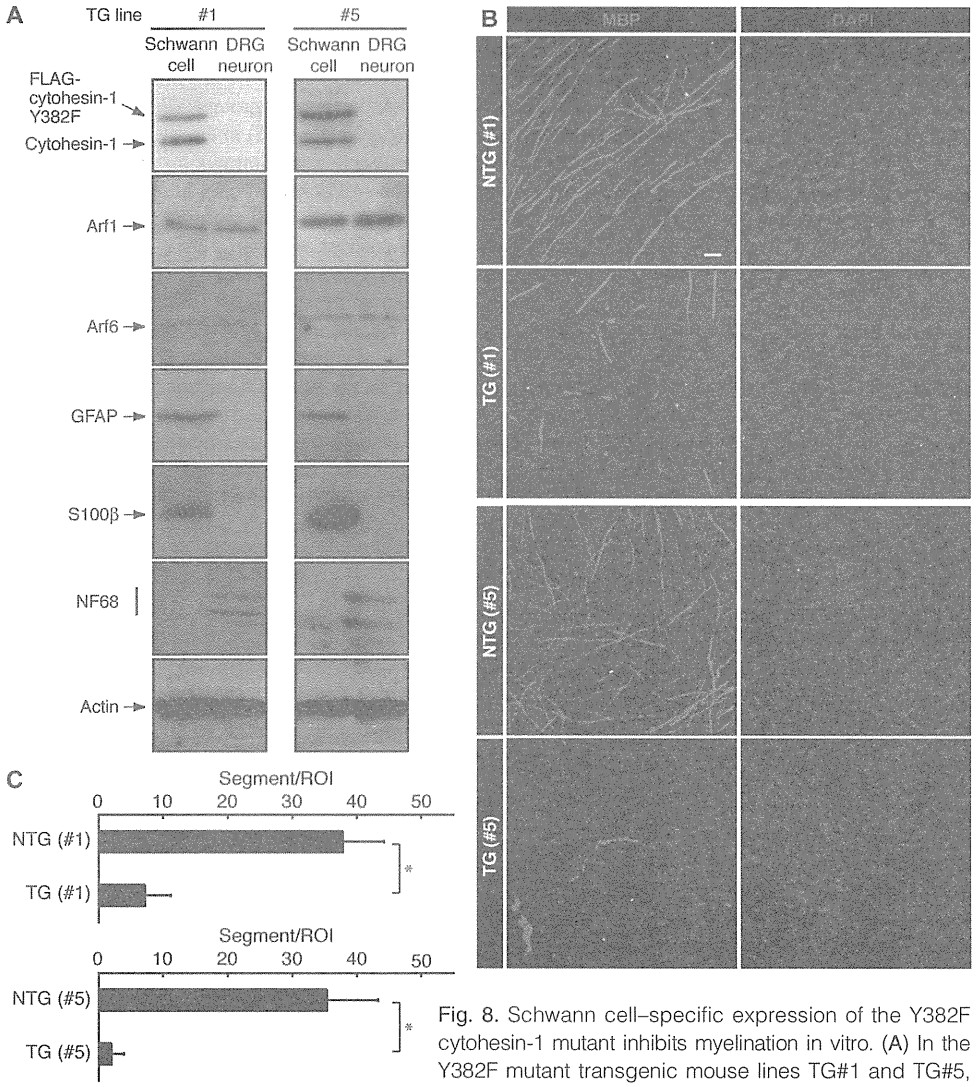

Fig. 8. Schwann cell–specific expression of the Y382F cytohesin-1 mutant inhibits myelination in vitro. (A) In the Y382F mutant transgenic mouse lines TG#1 and TG#5, specific expression of FLAG-tagged cytohesin-1 Y382F in Schwann cells, but not in DRG neurons, was confirmed by Western blotting analysis. The abundances of Schwann cell markers (GFAP and S100β), a neuronal marker (neurofilament 68 kD, NF68), and the Arf proteins were also determined. (B) Representative images of in vitro myelination from cultures established from transgenic mice (TG) and nontransgenic littermate controls (NTG). Cultures were stained with an anti-MBP antibody (red) and DAPI (blue). Scale bar, 20 μm. (C) The numbers of myelin segments were also determined. Data were evaluated by one-way ANOVA (*$P < 0.01$, $n = 5$ experiments).

were obtained in experiments with TG#5 mice and littermate controls (370 ± 20 myelinated axons compared to 380 ± 15, respectively), suggesting that the numbers of myelinated axons were comparable.

At an earlier postnatal stage (3 days), there was a difference in the number of myelinated axons between transgenic mice and their littermate controls. The number of myelinated axons was 120 ± 12 and 160 ± 16 in TG#1 mice and littermate controls, respectively. Similar results were obtained in experiments with TG#5 mice and littermate controls (127 ± 9.2 compared to 170 ± 18 myelinated axons). The average *g*-ratios in 3-day-old TG#1 mice were 0.81 ± 0.070, whereas littermate controls had *g*-ratios of 0.78 ± 0.072 (fig. S18, A and B). For 3-day-old TG#5 mice, the average *g*-ratios were 0.83 ± 0.053, whereas littermate controls had *g*-ratios of 0.78 ± 0.051 (fig. S18, C and D). Furthermore, the average *g*-ratios in 2-month-old TG#1 mice were 0.72 ± 0.059 compared to 0.67 ± 0.056 in littermate controls (fig. S18, A and B). For 2-month-old TG#5 mice, the average *g*-ratios were 0.71 ± 0.058 compared to 0.69 ± 0.049 in littermate controls (fig. S18, C and D). Although the involvement of Tyr^{382} phosphorylation in myelination was more pronounced at an early postnatal stage, these results indicated that cytohesin-1 and its phosphorylation at Tyr^{382} were required for proper myelination. The size distribution of the axons and axon sorting in the genetically modified mice and their littermate controls were apparently unaffected (Figs. 6C and 9B and figs. S14A and S18, A and C).

DISCUSSION

Phosphorylation of cytohesin-1 by Fyn is required for myelination by Schwann cells

In the series of processes involved in myelination, Schwann cells exhibit their characteristic ability to undergo continuous and dynamic morphological changes. Although many intercellular signals regulate myelination by Schwann cells, including growth factors derived from neurons and their cognate receptors on Schwann cells and vice versa (*1*–*4*), the nature of the intracellular signals in Schwann cells that are controlled by these intercellular signals is still largely unclear. Here, we demonstrated that cytohesin-1 promoted myelination of axons by Schwann cells through downstream activation of Arf6. We found that deletion of *cytohesin-1*, as well as inhibition of cytohesin-1 by the chemical inhibitor SecinH3, decreased myelination in cultured systems. *Cytohesin-1*$^{-/-}$ mice exhibited decreased myelin thickness compared to that of wild-type mice. In addition, we found that Fyn directly bound to and activated cytohesin-1 by phosphorylating Tyr^{382}. Transgenic mice expressing the Y382F mutant cytohesin-1 also exhibited decreased myelin thickness. These results support our previous hypothesis that cytohesin-1, whose tyrosine phosphorylation we found to be critical for triggering Schwann cell activation, played a key role in the process of myelination by Schwann cells. Further studies on the molecular mechanism controlling cytohesin-1 in the processes involved in myelination may help to promote our understanding of whether and how cytohesin-1 is physiologically associated with other GEFs or GAPs in a spatiotemporal manner.

Possible alternative role and regulatory mechanism of cytohesin-1 in Schwann cell myelination

The function of cytohesin-1 in lymphocytes has been well established (*12*, *13*, *16*, *17*). Cytohesin-1 is the binding partner of the intracellular region of the leukocyte-specific β_2 integrins, such as lymphocyte

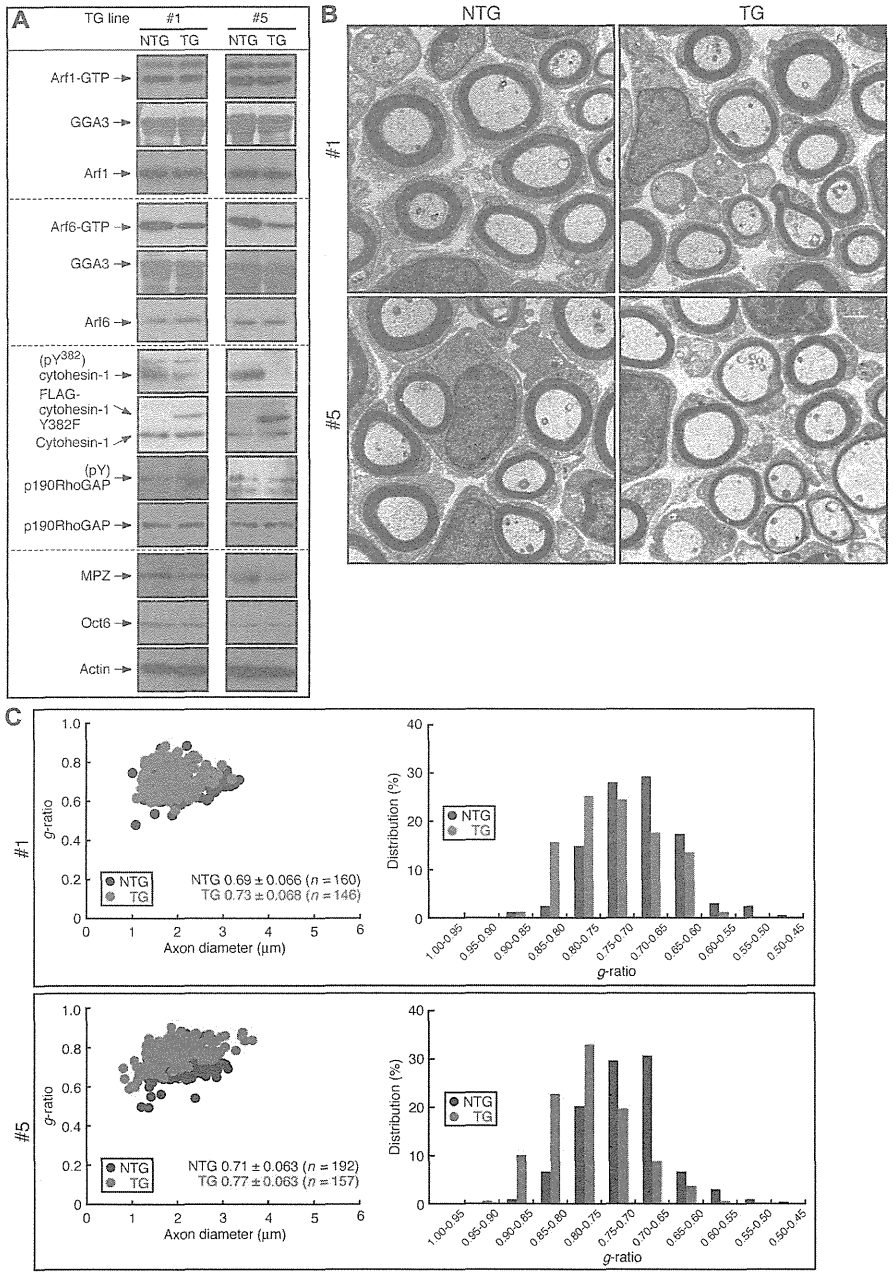

Fig. 9. Transgenic mice exhibit decreased myelin thickness in sciatic nerves. (A) Affinity precipitation assay of active Arf1 or Arf6 was performed with sciatic nerve extracts from 8-day-old TG#1 and TG#5 mice. Cell lysates were immunoprecipitated with an antibody against cytohesin-1 or p190RhoGAP and were analyzed by Western blotting with an antibody against (pY^{382})cytohesin-1 or pY. In addition, the abundances of cytohesin-1, p190RhoGAP, Arf1, Arf6, and other marker proteins were determined. Data are representative of four experiments. (B) Representative electron micrographs of five cross-sections of sciatic nerves from 8-day-old transgenic (TG) mice and nontransgenic littermate controls (NTG). Scale bar, 1 μm. (C) The *g*-ratios of the axons analyzed in (B) are plotted for each axon size. The average *g*-ratios are shown in the scatter plots on the left (n = 146 and 160 experiments for TG#1 mice and littermate controls, respectively; n = 157 and 192 experiments for TG#5 mice and littermate controls, respectively). Data are also presented in the form of relative distributions of the *g*-ratios in the bar graphs on the right.

function–associated antigen 1 (LFA-1). Binding of cytohesin-1 to LFA-1 is necessary for modulation of the inside-out signaling of β_2 integrins, but it does not require the GEF activity of cytohesin-1 (*16*). Whereas cytohesin-1 participates in controlling lymphocyte adhesion to cells expressing the integrin ligand intercellular adhesion molecule 1 (ICAM-1) and activating lymphocytes, only the latter process requires its GEF activity and the downstream activation of Arf6 (*17*). In Schwann cells, signals through integrins are indispensable for myelination (*4*, *35*). These signals are mediated by the integrin $\alpha_6\beta_1$ before the initiation of myelination and by the integrin $\alpha_6\beta_4$ during myelination. However, it seems unlikely that cytohesin-1 would bind directly to the β_1 or β_4 integrin subunits, given that it shows specific binding ability to the β_2 integrin subunit (*16*, *17*).

Cytohesin-family GEFs participate in inducing the enhanced phosphorylation of ErbB receptor tyrosine kinases, which is associated with some pathological states (*36*). In this case, cytohesin-2 and the epidermal growth factor receptor (EGFR; also known as ErbB1) are the main contributing factors. Cytohesin-2 binds to the intracellular region of the EGFR to initiate receptor transactivation, leading to enhanced receptor phosphorylation, which requires cytohesin-2 to undergo conformational changes but does not require its GEF activity. Because ErbB2 and ErbB3 play key roles in myelination (*2*, *3*), cytohesin-1 may be involved in their enhanced phosphorylation, but the details involved are currently unknown.

The mechanism whereby tyrosine phosphorylation activates a GEF for Rho GTPases is well characterized (*28*, *29*, *37*). The molecular mechanism involved in the activation of the RhoA-specific GEF Vav is particularly well studied (*38*). Vav contains an autoinhibitory helical region in tandem with the catalytic Dbl homology (DH) domain, and this autoinhibitory region is released upon its tyrosine phosphorylation, which in turn activates RhoA. A similar mechanism is probably conserved in the case of the activation of cytohesin-1. We found that cytohesin-1 was phosphorylated at Tyr^{382} and that this event was crucial for its GEF activity. This finding was supported by our modeling of cytohesin-1, which was constructed on the basis of the steric structure of cytohesin-3 (*30*). Our modeling predicts that Tyr^{382} exists in the C-terminal autoinhibitory helical region, which is structurally positioned above the catalytic Sec7 domain. Tyr^{382} phosphorylation may release the C-terminal region from the catalytic

domain and render Arf6 available for guanine nucleotide exchange. Although the entire 3D structure of cytohesin-1 has not been resolved, cytohesin-1 can be added to the list of GEFs that are directly activated by tyrosine phosphorylation. The tyrosine phosphorylation event might be one of the mechanisms that activate Arf GEFs as well as Rho GEFs, both of which are involved in the regulation of cell morphological changes, including those in Schwann cells (*7*, *31*).

Cytohesin-1 is potentially involved in the regulation of Schwann cell morphogenesis

Arf6 is a unique protein among the Arf family members. The major cellular role of Arf6 is to mediate morphological changes through cytoskeletal rearrangements, which is in contrast to the roles of the other Arfs, which are primarily involved in membrane dynamics (*10*, *11*). Regulation of morphological changes by Arf6 is mediated by the direct activation of a number of downstream effectors rather than indirectly by activation of a transcriptional factor. For example, Arf6 stimulates the enzymatic activities of effector proteins such as phospholipase D enzymes and phosphatidylinositol 4-phosphate 5-kinases. These enzymes generate certain phospholipid products that are incorporated into the regulatory proteins of the actin cytoskeleton, where they initiate morphological changes. Arf6 also regulates the tubulin cytoskeleton through effector proteins such as c-Jun N-terminal kinase–interacting protein 3 (JIP3) and JIP4 (*39*). JIP3 or JIP4 forms a complex with kinesin-1 and dynactin to control microtubule-dependent processes that in turn regulate morphological changes. Because myelination requires dynamic morphological changes, it is conceivable that these effector proteins may cooperatively act downstream of cytohesin-1.

Here, we demonstrated that activation of cytohesin-1 regulated myelination by Schwann cells and that cytohesin-1 activation occurred through its direct tyrosine phosphorylation by Fyn, thus illustrating a possible mechanism underlying the activation of small GTPases. Further studies on the role and regulation of cytohesin-1 will enhance our understanding of the precise mechanism by which Fyn and cytohesin-1 regulate myelination and whether cytohesin-1 specifically transduces signals from axonal cues such as NRG1 type III (*3*).

MATERIALS AND METHODS

Antibodies

The antibodies used in this study are listed according to source and include information on antibody type and the dilution at which the antibodies were used in Western blotting analysis. Anti-Arf1 (polyclonal, 1:1000) and anti-Arf6 (monoclonal, 1:1000) were from Sigma-Aldrich; anti-Arf1 (monoclonal, 1:20) and anti-Arf6 (monoclonal, 1:20) were from Santa Cruz Biotechnology; anti-Fyn (monoclonal, 1:50 for Western blotting and 1:25 for immunofluorescence) was from Santa Cruz Biotechnology; anti-Fyn (monoclonal, used at 1 μg per ~100 μg of cell lysate for immunoprecipitation) was from Millipore; anti-pY (monoclonal, 1:100), anti-Oct6 (polyclonal, 1:100), and anti-Krox20 (polyclonal, 1:100) were from Santa Cruz Biotechnology; anti–nerve growth factor (NGF) (monoclonal, used at 5 μg/ml for immunodepletion) was from Millipore; anti-MPZ (polyclonal, 1:50) was from Abnova; anti-MPZ (polyclonal, 1:100) was from Medical and Biological Laboratories; anti-MBP (monoclonal, 1:100 for immunofluorescence) and anti-GFAP (monoclonal, 1:500) were from Covance; anti-S100β (monoclonal, 1:500 for Western blotting, immunofluorescence, and immunohistochemistry) was from Abcam; anti–neurofilaments 68 and 160/200 (monoclonal, 1:1000 for immunofluorescence and immunohistochemistry) were from Covance; anti–neurofilament 68 (monoclonal, 1:500) was from Cell Signaling Technology; anti-p190RhoGAP (polyclonal, 1:500), whose tyrosine phosphorylation is mediated by Fyn, was from Cell Signaling Technology; anti-actin (monoclonal, 1:500) was from BD Biosciences Pharmingen; anti-Ki67 (monoclonal, 1:500 for immunohistochemistry) was from Dako; anti-FLAG/DDDDK (monoclonal, 1 μg/ml for Western blotting and 1 μg per ~100 μg of cell lysate for immunoprecipitation) was from Sigma-Aldrich; anti-DDDDK/FLAG (monoclonal and polyclonal, 1:1000 for Western blotting and immunofluorescence) was from Medical and Biological Laboratories; anti-V5 (monoclonal, 1:1000) was from Nacalai Tesque and Wako; anti-His (monoclonal, 1:1000) was from Medical and Biological Laboratories; anti-(pY^{416})panSrc (polyclonal, 1:500 for Western blotting and 1:250 for immunofluorescence), which recognizes an autophosphorylation site common to members of the Src family, was from Santa Cruz Biotechnology; and anti-(pY^{527})panSrc (polyclonal, 1:500), which recognizes an inhibitory phosphorylation site common to members of the Src family, was from Cell Signaling Technology. The amino acid residue 527 in Src corresponds to amino acid residue 531 in Fyn. Peroxidase-conjugated secondary antibodies were obtained from GE Healthcare and Immuno-Biological Laboratories. Fluorescently labeled secondary antibodies were obtained from Life Technologies and Immuno-Biological Laboratories. Secondary antibodies were used according to the respective manufacturers' instructions. Rabbit antiserum specific for cytohesin-1 was generated against the peptide MEDDDSYVPSDLTAE (synthesized by Iwaki) and affinity-purified with a peptide-conjugated resin. The antiserum was used at a concentration of 1.5 μg/ml for Western blotting, 3 μg/ml for immunofluorescence and immunohistochemistry, and 1 μg per ~100 μg of cell lysate for immunoprecipitation studies. Rabbit antiserum specific for (pY^{382})cytohesin-1 was generated against the phosphorylated peptide RDPFpYEMLAA (synthesized by Medical and Biological Laboratories). The antiserum was affinity-purified with a phosphorylated peptide–conjugated resin from nonabsorbed fractions of a nonphosphorylated peptide–conjugated resin. This antiserum was used at a concentration of 15 μg/ml for Western blotting analysis and 30 μg/ml for immunofluorescence studies.

RT-PCR and DNA primers

Total RNA was extracted with TRIzol reagent (Life Technologies). The complementary DNAs (cDNAs) were prepared from 1 μg of total RNA with SuperScript III reverse transcriptase (Life Technologies) according to the manufacturer's instructions. PCR amplification was performed with ExTaq DNA polymerase at 30 cycles, each consisting of denaturation at 94°C for 1 min, annealing at 59.5°C for 1 min, and extension at 72°C for 1 min. The DNA primers were synthesized by Fasmac. The primers used were 5′-ATGGAGGACGATGACAGCTATG-3′ (sense) and 5′-GACAGTACCGCTGCGCAAAG-3′ (antisense) for rat cytohesin-1; 5′-ATGGAGGACGGTGTCTACGAG-3′ (sense) and 5′-GGATTACATAAGCAATATCTCTGGGCAAAG-3′ (antisense) for rat cytohesin-2; 5′-ATGGACGAAGGCGGTGGC-3′ (sense) and 5′-GACGCAAAGGCCTCCATCATG-3′ (antisense) for rat cytohesin-3; 5′-ATGGATGTATGTCATGCAGATACAGCTG-3′ (sense) and 5′-ACAGAGGCAGTAGCGAGCAG-3′ (antisense) for rat cytohesin-4; 5′-ATGGGCTGTGTGCAATGTAAGGATAAAGAAG-3′ (sense) and 5′-GATAAGAAAGGTACCTCTTGGGTTTCCAAAGGAC-3′ (antisense) for rat Fyn; 5′-ATGGGATGTATTAAATCAAAAAGGAAAGACAATCTGAATGAC-3′ (sense) and 5′-CATAGGGTCGTAATCTCTGACGGAAAGAGAG-3′ (antisense) for rat Lyn; 5′-ATGGGCAGCAACAAGAGCAAGC-3′ (sense) and 5′-GGCGTTGAGAAGTAGCCGCTCTG-3′ (antisense) for rat Src (c-Src); 5′-ATGGGCTGCATTAAAAGTAAAGAAAACAAAAGTCCAG-3′ (sense) and 5′-ATTCCCAGGATTCAGAAGTAATCTTTCAGCATC-3′ (antisense) for rat Yes; 5′-ATGGGGCTACTGAGCAGCAAGAG-3′ (sense) and 5′-TGAGCGGATCTTATAGTGCTTGACCATC-3′ (antisense) for rat Blk; 5′-ATGGGCTGTGTGTTCTGCAAGAAGTTAG-3′ (sense) and 5′-CCAGTCACGGATGGACAGGGAG-3′ (antisense) for rat Fgr;

5′-CTGGGGGGTCGTTCGAGCTG-3′ (sense) and 5′-TTTGGTGGTCTCACTGTCCCGGATC-3′ (antisense) for rat Hck; and 5′-ATGGGCTGTGTCTGCAGCTCAAAC-3′ (sense) and 5′-TCCCTGGTTCTGGTCGAAGTCTCTG-3′ (antisense) for rat Lck. The control primers for rodent β-actin were 5′-ATGGATGACGATATCGCTGCGCTC-3′ (sense) and 5′-CTAGAAGCATTTGCGGTGCACGATG-3′ (antisense).

Cultures of primary DRG neurons

Rodents (rats and genetically modified or unmodified mice) were cared for in accordance with the protocol approved by the Japanese National Research Institute for Child Health and Development Animal Care Committee and were monitored by the Laboratory Animal Facility of the Japanese National Research Institute for Child Health and Development. Primary neurons were dissociated from DRGs of C57BL/6JJms mouse or Sprague-Dawley rat embryos on embryonic day 13 or 15 (Sankyo Laboratories) and were purified by culturing on collagen-coated dishes or wells in Dulbecco's modified Eagle's medium (DMEM)–GlutaMAX I (Life Technologies) containing 10% fetal bovine serum (FBS), NGF (100 ng/ml), 8 μM fluorodeoxyuridine, and 4 μM uridine in 95% humidified air and 5% CO_2 (*40*). After three cycles of antimitotic reagent administration over 2 to 3 weeks, purified DRG neurons were cultured in DMEM–GlutaMAX I containing 10% FBS and NGF (100 ng/ml). Medium used in culture without antimitotic reagents for 2 to 3 days was collected as DRG neuronal CM and stored at −80°C until required.

Primary Schwann cell culture

Primary Schwann cells were prepared from the sciatic nerves of male or female rats or mice on postnatal day 1, as previously described (*40*). Briefly, Schwann cells were cultured on polylysine-coated dishes in DMEM containing 10% heat-inactivated FBS, gentamicin (50 μg/ml), and 10 μM arabinosylcytosine at 37°C in 95% humidified air and 5% CO_2. After 2 to 3 days, Schwann cells were detached from dishes with 0.05% trypsin and were cultured in DMEM containing 10% FBS and gentamicin (50 μg/ml). Schwann cells were plated for experiments on collagen-coated dishes or wells in Sato medium containing bovine serum albumin (BSA; 1 mg/ml). Unless otherwise indicated, Schwann cells were treated with or without neuronal CM containing anti-NGF antibody (5 μg/ml), NRG1 (R&D Systems), or IGF-1 (Life Technologies) in the presence or absence of 10 μM SecinH3 (Merck) for 30 min. SecinH3 is a specific inhibitor of cytohesin-family GEFs. To confirm cell viability under these experimental conditions, we stained Schwann cells with 0.4% trypan blue. Attached cells incorporating trypan blue made up less than 5% of the cells in each experiment.

Cell line culture

HEK 293T cells and a rat immortalized Schwann cell line (RT4-D6P2T) were cultured on dishes in DMEM containing 10% FBS, penicillin (50 U/ml), and streptomycin (50 μg/ml).

In vitro myelination

Dissociated explants were established from mice on embryonic day 13 (*20*). Briefly, DRGs were collected and dissociated with 0.25% trypsin and trituration. Cells were dispersed and plated onto collagen-coated coverslips (3×10^5 cells per coverslip). The dissociated explants were maintained in minimum essential medium containing 10% FBS and NGF (100 ng/ml). Axonal processes and endogenous Schwann cells were allowed to grow and establish themselves for 5 days. Myelination was then induced with ascorbic acid (50 μg/ml). Culture medium was changed every 2 to 3 days, and cultures were maintained for an additional 13 to 15 days. Cocultures of rat Schwann cells and DRG neurons were also established as previously described (*20*). For statistical analysis, the myelin segments in a 200-μm^2 field were counted.

Small interfering RNAs

The small interfering RNA (siRNA) duplexes were synthesized by Eurogentec. The nucleotide target sequences were 5′-AAGATTGACCGGATGATGGAG-3′ for rat cytohesin-1 (siCytohesin-1) and 5′-AACTACAACAACTTCCACGCA-3′ for rat Fyn (siFyn). The target sequence of the control *Photinus pyralis* luciferase was 5′-AAGCCATTCTATCCTCTAGAG-3′. The luciferase siRNA target sequence does not have homology to any other mammalian gene sequences. Rat Schwann cells were transfected with the siRNAs (100 ng of total RNA for 2×10^5 cells) with PrimaPort reagent (Wako) or a Nucleofector II device (Lonza) with the Basic Neuron Nucleofector kit (Lonza), according to the respective manufacturers' instructions. The culture medium was replaced with Sato medium at 24 hours after transfection. Attached cells incorporating trypan blue made up less than 5% of the cells 48 hours after transfection.

Plasmids

Gene recombination was performed in accordance with the protocol approved by the Japanese National Research Institute for Child Health and Development Gene Recombination Committee. The coding region of mouse full-length cytohesin-1 (also referred to as mKIAA4240), which was provided by H. Koga (Kazusa DNA Research Institute, Chiba, Japan), was ligated into the mammalian expression vector p3×FLAG-myc-CMV-24 (pCMV-FLAG, Sigma-Aldrich). The cytohesin-1 cDNA fragments encoding the CC region (CC, amino acid residues 1 to 52), the Sec7 domain (Sec7, amino acid residues 53 to 255), and the PH domain with the C-terminal region (PH, amino acid residues 256 to 398) were inserted into pCMV-FLAG. The isolated Sec7 domain exhibits constitutively active GEF activity (*30*). The PH domain was also inserted into the pCMV vector containing the myc epitope at the 5′ position and into pET42a vector (EMD Biosciences). The PH domain construct harboring the Y291F, Y292F, Y295F, Y327F, Y355F, or Y382F mutations was produced according to the overlapping PCR method and ligated into pCMV-FLAG. cDNA encoding full-length cytohesin-1 harboring the Y382F mutation was also produced according to the overlapping PCR method and ligated into pCMV-FLAG. The region encoding Arf6 (amino acid residues 13 to 175), a deleted series of 12 hydrophobic amino acids at the N terminus (*30*), was amplified from total RNA of human brain by RT-PCR and was ligated into the *Escherichia coli* His- and glutathione *S*-transferase (GST)–tagged expression vectors pET28a and pET42a, respectively. The mammalian expression plasmids pME18S-Fyn and pME18S-FynY531F (a constitutively active form of Fyn) (*19*) were provided by T. Yamamoto (Tokyo University, Tokyo, Japan and Okinawa Institute of Science and Technology Graduate University, Okinawa, Japan) and T. Tezuka (Tokyo Medical and Dental University, Tokyo, Japan). The cDNA fragments encoding the SH4 domain (amino acids 1 to 83), SH3 domain (amino acids 84 to 143), SH2 domain (amino acids 144 to 263), and SH1 domain (the kinase domain, amino acids 264 to 537) were amplified from pME18S-Fyn and inserted into the pCMV vector containing the V5 epitope at the 3′ position. The pET42a-GGA3 plasmid (amino acids 1 to 343) was constructed as previously described (*41*). All DNA sequences were confirmed with an automated DNA sequencer (Life Technologies). HEK 293T and RT4-D6P2T cells (2 μg of total DNA for 1×10^6 cells) were transfected with CalPhos reagent (Takara Bio) or Lipofectamine-Plus reagent (Life Technologies) according to the respective manufacturers' instructions.

Immunoprecipitation and Western blotting analysis

Cells were lysed in lysis buffer A [50 mM Hepes-NaOH (pH 7.5), 20 mM $MgCl_2$, 150 mM NaCl, 1 mM dithiothreitol (DTT), 1 mM phenylmethylsulfonyl fluoride (PMSF), leupeptin (1 μg/ml), 1 mM EDTA, 1 mM Na_3VO_4, 10 mM NaF, and 0.5% NP-40] for extraction of cytoplasmic

and membrane fractions or in lysis buffer A containing 1% CHAPS and 0.3% SDS for extraction of nuclear fractions. Unless otherwise indicated, all steps in the immunoprecipitation process and the protein purification process were performed at 4°C. For immunoprecipitations, the supernatants cleared by centrifugation (200 μg of total protein for cell line and tissue extracts; 100 μg of total protein for primary cell extracts) were mixed with an antibody-absorbed protein G resin (GE Healthcare) or ExactaCruz (Santa Cruz Biotechnology) according to the respective manufacturers' instructions. The immunoprecipitates or proteins in the cell supernatants were denatured and then subjected to SDS-PAGE. The electrophoretically separated proteins were transferred onto a polyvinylidene difluoride membrane, blocked with Blocking One reagent (Nacalai Tesque) according to the manufacturer's instructions, and incubated with a primary antibody and then with a peroxidase-conjugated secondary antibody. The bound antibodies were detected with chemiluminescence reagent (GE Healthcare).

Recombinant proteins

HEK 293T cells were transiently transfected with the plasmid encoding FLAG-tagged wilt-type cytohesin-1 or the Y382F mutant and were cultured in serum-containing medium for 24 hours and then serum-starved for 24 hours. Cells were collected and lysed with lysis buffer A. Supernatants were cleared by centrifugation and then were mixed with a protein G resin absorbed with an anti-FLAG antibody, washed with lysis buffer A containing 500 mM NaCl and then with lysis buffer A containing 500 mM NaCl and 50 mM EDTA, and eluted with lysis buffer A containing 20 mM FLAG peptide (Sigma-Aldrich) according to the manufacturer's instructions. The buffer contained in the eluted fractions was exchanged with reaction buffer A [20 mM Hepes-NaOH (pH 7.5), 5 mM $MgCl_2$, 150 mM NaCl, 1 mM DTT, 1 mM PMSF, leupeptin (1 μg/ml), and 1 mM EDTA]. Aliquots were stored at −80°C until required. Recombinant His-tagged Fyn protein was purchased from Millipore. Recombinant His- or GST-tagged Arf6, GST-tagged PH domain of cytohesin-1, and GST-tagged GGA3 were expressed in *E. coli* BL21 (DE3) pLysS. Briefly, transformed *E. coli* cells were treated with 0.4 μM isopropyl-1-thio-β-D-galactopyranoside at 30°C for 2.5 hours and then harvested. The cell precipitates were extracted with extraction buffer A [50 mM tris-HCl (pH 7.5), 5 mM $MgCl_2$, 1 mM DTT, 1 mM PMSF, leupeptin (1 μg/ml), 1 mM EDTA, and 0.5% NP-40] containing lysozyme (500 μg/ml) and deoxyribonuclease I (100 μg/ml). Supernatants cleared by centrifugation were mixed with nickel or glutathione resin. The bound proteins were washed with extraction buffer A and eluted with extraction buffer A containing 200 mM imidazole (for the nickel resin) or 20 mM glutathione (for the glutathione resin) according to the respective manufacturers' instructions. The buffer contained in the elution fractions was exchanged with reaction buffer A for recombinant proteins other than Arf6 or with reaction buffer A containing 0.1 μM GDP for Arf6.

Detection of active Arf1 and Arf6

To detect active GTP-bound forms of Arf1 and Arf6 in cell lysates, affinity precipitation was performed with GST-GGA3 (*21*, *22*). The affinity-precipitated Arf1 or Arf6 was detected by Western blotting with an antibody against Arf1 or Arf6. For comparison of the amounts of recombinant GST-GGA3 proteins, GGA3 loaded under the same conditions was also stained with 0.25% Coomassie Brilliant Blue R-250.

Detection of active cytohesin-1

To detect active cytohesin-1 in cell lysates, we performed affinity precipitation with GST-tagged, guanine nucleotide–free Arf6. Catalytically active GEFs preferentially interact with nucleotide-free GTPases (*27*–*29*). The affinity-precipitated cytohesin-1 was detected by Western blotting with an antibody against cytohesin-1. For comparison of the amounts of recombinant GST-Arf6 proteins, Arf6 loaded under the same conditions was also stained with Coomassie Brilliant Blue.

MS-based identification of a cytohesin-1–binding protein

RT4-D6P2T cells (1×10^9) were left untransfected or were transiently transfected with plasmid encoding the myc-tagged PH domain of cytohesin-1. Forty-eight hours later, cells were lysed in lysis buffer A. Protein complexes containing the PH domain were isolated from cleared supernatants with a myc-tagged Protein Mild Purification Kit (Medical and Biological Laboratories) according to the manufacturer's instruction. Fractions containing the complexes were filtered through a 30,000 molecular weight cutoff membrane (Millipore), subjected to SDS-PAGE, and visualized by silver staining. Protein bands were excised and enzymatically digested in-gel as previously described (*42*). The resultant peptides were analyzed with an Ettan MALDI-TOF Pro mass spectroscope (GE Healthcare) and a Mascot database (Matrix Science Inc.).

In vitro binding assay of Fyn and cytohesin-1

His-tagged Fyn protein (17 to 2200 nM) was mixed with immobilized FLAG-tagged cytohesin-1 (30 μg) in 60 μl of reaction buffer A at 4°C for 2 hours. The resin was washed with reaction buffer A, subjected to SDS-PAGE, and analyzed by Western blotting with an anti-His antibody. The binding of Fyn to cytohesin-1 was measured on the basis of band intensities, which were analyzed with UN-SCAN-IT software (Silk Scientific Inc.). The K_d value was calculated by the Scatchard analysis (*41*).

In vitro kinase assay of Fyn

Immunoprecipitated Fyn proteins were incubated with 5 μg of recombinant GST-tagged PH domain, as the substrate, and 20 μM adenosine 5′-triphosphate (ATP) in 30 μl of reaction buffer A at 30°C for 30 min. Samples were then diluted with ice-cold reaction buffer A and chilled on ice. After centrifugation, the GST-PH domain was collected from the supernatant with glutathione resin. The tyrosine-phosphorylated PH domain was detected by Western blotting with an anti-pY antibody. For comparison of the amounts of recombinant GST-PH domain proteins, samples of PH domain loaded under the same conditions were also stained with Coomassie Brilliant Blue.

In vitro tyrosine phosphorylation reaction of cytohesin-1

Purified immobilized FLAG–cytohesin-1 proteins (100 ng) or immunoprecipitates were incubated with 20 μM cold ATP in the presence or absence of 100 ng of recombinant Fyn in 30 μl of reaction buffer A at 30°C for 30 min and then were chilled on ice (*7*). Immobilized proteins were washed with reaction buffer A and used for Western blotting analysis and guanine nucleotide–releasing assays.

Guanine nucleotide exchange assay

Guanine nucleotide–binding and guanine nucleotide–releasing reactions were measured. The binding assay is more direct than the releasing assay (*30*, *43*). For guanine nucleotide–binding assays, immobilized cytohesin-1 proteins (100 ng) were incubated in 30 μl of reaction buffer B [20 mM Hepes-NaOH (pH 7.5), 1 mM $MgCl_2$, 1 mM DTT, 1 mM PMSF, leupeptin (1 μg/ml), and 2 mM EDTA] containing His-Arf6 (16 ng/μl) and 4 μM mant-GTP (Life Technologies) at 30°C. Changes in mant-GTP fluorescence (excitation, 360 nm; emission, 440 nm) were analyzed with an Infinite M200 microplate reader system (Tecan Systems). Representative data of three experiments are shown in the figure. For guanine nucleotide–releasing assays, [^{3}H]GDP-bound His-Arf6 was obtained by incubation with reaction buffer A containing His-Arf6 (125 ng/μl), BSA (250 ng/μl), and

0.3 mM [^{3}H]GDP (0.3 μCi/μl) at 30°C for 90 min, followed immediately by chilling on ice. Immobilized cytohesin-1 proteins (100 ng) were incubated in 30 μl of reaction buffer A containing [^{3}H]GDP-occupied His-Arf6 (16 ng/μl), BSA (33 ng/μl), and 10 μM cold GTPγS at 30°C for 30 min (*7*). The reaction solution was immediately filtered through a 0.45-μm nitrocellulose membrane. The membranes were washed with ice-cold reaction buffer A and air-dried. The radioactivity remaining in each membrane was measured with a liquid scintillation counter (Hitachi-Aloka Medical).

Generation of knockout mice

A 13.5-kb Xba I fragment of genomic DNA containing exons 4 to 11 of *cytohesin-1* was obtained from a 129/Sv mouse genomic library (*18*). The *cytohesin-1*–targeting vector was constructed by replacing the ~3.6-kb Xba I fragment containing exons 4 to 7 of *cytohesin-1* within the fragment containing exons 4 to 11, which was ligated to the gene encoding diphtheria toxin, with a cassette of the neomycin-resistant gene (*44*). 129/Sv embryonic stem (ES) cells were transfected with the linearized targeting vector by electroporation. G418-resistant, homologous recombination–positive transfectants were identified by genomic PCR analysis. The primers used for genomic PCR were 5′-AACAAGACAGCCATCGGCGACTAC-3′ (sense) and 5′-CACAAACGCATGCAGGACCTGGATG-3′ (antisense) for wild-type *cytohesin-1*, 5′-CCCGGTTCTTTTTGTCAAGACCGACCTGTC-3′ (sense) and 5′-CATTCGCCGCCAAGCTCTTCAGCAATATCAC-3′ (antisense) for *neo*, and 5′-AAGCTTTGTGAACTTGGCGGCTTCCAAGTCG-3′ (sense) and 5′-CATTACTGGCCTGGTGCTTAGTTATCTTTG-3′ (antisense) for *oct3/4* as the control amplification. PCR amplification was performed in 30 cycles, each consisting of denaturation at 94°C for 1 min, annealing at 68°C for 1 min, and extension at 72°C for 1 min. These ES cells were used to generate chimeric mice. Offspring were genotyped by means of genomic PCR and Southern blotting with Eco RI–digested tail DNA hybridized to a genomic probe for a ~0.5-kb Eco RI–Xba I position between exons 3 and 4. The wild-type *cytohesin-1* allele resulted in a hybridized band of ~7.0 kb, whereas the knockout allele resulted in a hybridized band of ~4.6 kb. Heterozygous offspring were mated to wild-type C57BL/6JJms mice, and the mutations were propagated in this strain for at least 10 generations before it was crossed to produce homozygotes for experiments. Homozygous mice, as well as heterozygous mice, were fertile under standard breeding conditions. Fyn-knockout mice (on a mixed 129/Sv × C57BL/6J background) were obtained from The Jackson Laboratory. Heterozygous offspring were mated to wild-type C57BL/6JJms mice, and the mutations were propagated in this strain for at least five generations before it was crossed to produce homozygotes for experiments. The genomic PCR for identification of the knockout allele was performed according to The Jackson Laboratory's standard protocol. Male mice were used for experiments if it was possible to distinguish their sex.

Transgenic mice

The mouse *gfap* promoter and a MoMLV-derived artificial intron were amplified with the mammalian in vivo expression vector pDRIVE-mGFAP (17 to 1695 bases; InvivoGen) and the mammalian-retrovirus expression vector pMEI5 (901 to 1721 bases; Takara Bio), respectively, as templates. They were digested with the Bgl II and Bam HI restriction enzymes. The nucleotide units encoding the simian virus 40 (SV40) enhancer, the mouse *gfap* promoter, the FLAG-tagged Y382F mutant of cytohesin-1, the MoMLV intron, and the human growth hormone polyadenylate signal were successively inserted into a pCMV backbone as the subcloning vector. A DNA fragment (~5.1 kb) containing all nucleotide units was digested from the vector backbone with Nco I, purified, and injected into fertilized C57BL/6JJms oocytes. Transgenic founder mice and established transgenic mice (two lines: #1 and #5) were identified by means of tail genomic PCR with the specific primers 5′-CCGGAATTCGAATATTAGCTAGGAGTTTCAGAAAGGGGGCCTG-3′ and 5′-CCGGAATTCACTAGTGGGACTATGGTTGCTGACTAATTGAGATGC-3′ for the *sv40* enhancer and 5′-ATGGACTACAAAGACCATGACGGTGATTATAAAGATCATGACATCGAC-3′ and 5′-GTGTCTCTTTGTGGAGGAGACCTTCTTTTTCCGTG-3′ for *cytohesin-1*, and Southern blotting with Bgl II–digested tail DNA hybridized to a genomic probe for the MoMLV intron. The transgenic allele resulted in a hybridized band of ~3.1 kb. PCR was performed in 30 cycles, each consisting of denaturation at 94°C for 1 min, annealing at 65°C for 1 min, and extension at 72°C for 1 min. Transgenic founders were mated to wild-type C57BL/6JJms mice, and the transgene was stably maintained for at least five generations. The transgenic mice, as well as their nontransgenic littermates, were fertile under standard breeding conditions. Male mice were used for experiments if it was possible to distinguish their sex.

Chromosome preparation and fluorescence in situ hybridization

Chromosome preparation, replication of R-banding, and fluorescence in situ hybridization (FISH) mapping were performed according to the method of Matsuda and Chapman (*45*). Briefly, transgenic mouse splenocytes on glass slides were synchronized in the presence of thymidine for 16 hours and treated with 5-bromo-2′-deoxyuridine for an additional 5.5 hours. The cells were further treated with colcemid and harvested. The transgene DNAs were labeled with Cy3–deoxyuridine triphosphate for use as probes. After hybridization, the glass slides were washed first in a solution of 50% formamide and 2× SSC buffer and then in 1× SSC and counterstained with DAPI. FISH images were captured with a DMRA2 microscope system (Leica) and analyzed with CW4000 FISH software (Leica).

Immunofluorescence

Cells on collagen-coated glass coverslips were fixed in phosphate-buffered saline (PBS) containing 4% paraformaldehyde (PFA) and permeabilized with PBS containing 0.1% Tween 20. Before fixation, Schwann cells were left untreated or were treated with neuronal CM for 30 min. Permeabilized cells were blocked with Blocking One reagent and incubated first with primary antibodies and then with fluorescently labeled secondary antibodies. The glass coverslips were mounted with Vectashield reagent containing DAPI (Vector Laboratories) onto slides for microscopic observation. The fluorescent images were captured with an Eclipse TE-300 microscope system (Nikon) and analyzed with AxioVision software (Carl Zeiss) or were captured with a DMI4000 microscope system (Leica) and analyzed with AF6000 software (Leica). The confocal images were collected with an IX81 microscope with a laser-scanning FV500 or FV1000D system (Olympus) and analyzed with the respective FluoView software (Olympus).

Immunohistochemistry

Tissues were perfused first with PBS and then with PBS containing 4% PFA. They were postfixed with 4% PFA, which was replaced with 20% sucrose, and then embedded in Tissue-Tek reagent (Sakura Finetechnical). Microtome sections on glass slides were blocked with Blocking One reagent and incubated first with primary antibodies and then with fluorescently labeled secondary antibodies. The glass slides were mounted with Vectashield reagent containing DAPI or EthD-2 (ethidium homodimer-2). Fluorescent images were captured with a DM2500 microscope system (Leica) and analyzed with LAS software (Leica) or with a BX51 microscope system (Olympus) and analyzed with DP2-BSW software (Olympus). For statistical analysis, the number of DAPI-positive cells in a 200-μm^2 field was counted. Both cross-sections and longitudinal sections of sciatic nerves

contained DAPI-positive cell bodies of Schwann cells, but neither type of section contained neuronal cell bodies.

EM analysis

Sciatic nerves were fixed with 2% glutaraldehyde and 2% PFA in 0.1% cacodylate buffer, contrasted with 2% osmium tetroxide, dehydrated with an ethanol gradient, and treated with propylene oxide. Finally, samples were infiltrated and embedded in pure epoxy. Ultrathin sections were stained with uranyl acetate and lead staining solution. Images were taken with a JEM-1200EX EM system (JOEL). For statistical analysis, the *g*-ratio, which is the numerical ratio between the diameter of the axon and the outer diameter of the myelinated fiber, was measured.

Molecular modeling

The model of mouse cytohesin-1 (amino acid residues 60 to 394) was generated on the basis of the structure of human cytohesin-3 (Protein Data Bank ID: 2R09) with MOE software (Ryoka System Inc.).

Statistical analysis

Values are presented as the means ± SD from separate experiments. A one-way ANOVA was followed by a Fisher's protected least significant difference test as a post hoc comparison.

SUPPLEMENTARY MATERIALS

www.sciencesignaling.org/cgi/content/full/5/243/ra69/DC1

Fig. S1. Analysis of cytohesin-1 localization in cocultures and sciatic nerves.
Fig. S2. Confirmation of the specificity of an affinity-purified antibody for cytohesin-1.
Fig. S3. Effects of neuronal CM on the expression of cytohesin-family GEFs.
Fig. S4. Specific precipitation of a constitutively active cytohesin-1 with guanine nucleotide–free Arf6.
Fig. S5. Estimation of a purified cytohesin-1 protein.
Fig. S6. Identification of the site in cytohesin-1 that is phosphorylated by Fyn.
Fig. S7. Binding of cytohesin-1 to the SH1 domain of Fyn.
Fig. S8. Confirmation of the specificity of an affinity-purified antibody against (pY^{382})cytohesin-1.
Fig. S9. Comparison of the amino acid sequences of cytohesin-family GEFs.
Fig. S10. Estimation of purified Y382F mutant and Arf6 proteins and the guanine nucleotide–releasing assay.
Fig. S11. Generation of *cytohesin-1*$^{-/-}$ mice.
Fig. S12. Analysis of the abundances of Oct6 and Krox20 in sciatic nerves from *cytohesin-1*$^{-/-}$ mice.
Fig. S13. Analysis of cell numbers in sciatic nerves from *cytohesin-1*$^{-/-}$ mice.
Fig. S14. EM analysis of sciatic nerves from *cytohesin-1*$^{-/-}$ mice.
Fig. S15. Generation of transgenic mice (TG#1 and TG#5) of the Y382F mutant.
Fig. S16. Analysis of the abundances of Oct6 and Krox20 in transgenic mice.
Fig. S17. Analysis of cell numbers in sciatic nerves from transgenic mice.
Fig. S18. EM analysis of sciatic nerves from transgenic mice.

REFERENCES AND NOTES

1. R. P. Bunge, Expanding roles for the Schwann cell: Ensheathment, myelination, trophism and regeneration. *Curr. Opin. Neurobiol.* **3**, 805–809 (1993).
2. R. Mirsky, K. R. Jessen, Schwann cell development, differentiation and myelination. *Curr. Opin. Neurobiol.* **6**, 89–96 (1996).
3. K. A. Nave, J. L. Salzer, Axonal regulation of myelination by neuregulin 1. *Curr. Opin. Neurobiol.* **16**, 492–500 (2006).
4. C. Taveggia, M. L. Feltri, L. Wrabetz, Signals to promote myelin formation and repair. *Nat. Rev. Neurol.* **6**, 276–287 (2010).
5. Y. Benninger, T. Thurnherr, J. A. Pereira, S. Krause, X. Wu, A. Chrostek-Grashoff, D. Herzog, K. A. Nave, R. J. Franklin, D. Meijer, C. Brakebusch, U. Suter, J. B. Relvas, Essential and distinct roles for cdc42 and rac1 in the regulation of Schwann cell biology during peripheral nervous system development. *J. Cell Biol.* **177**, 1051–1061 (2007).
6. A. Nodari, D. Zambroni, A. Quattrini, F. A. Court, A. D'Urso, A. Recchia, V. L. Tybulewicz, L. Wrabetz, M. L. Feltri, β1 integrin activates Rac1 in Schwann cells to generate radial lamellae during axonal sorting and myelination. *J. Cell Biol.* **177**, 1063–1075 (2007).
7. J. Yamauchi, Y. Miyamoto, J. R. Chan, A. Tanoue, ErbB2 directly activates the exchange factor Dock7 to promote Schwann cell migration. *J. Cell Biol.* **181**, 351–365 (2008).
8. N. Novak, V. Bar, H. Sabanay, S. Frechter, M. Jaegle, S. B. Snapper, D. Meijer, E. Peles, N-WASP is required for membrane wrapping and myelination by Schwann cells. *J. Cell Biol.* **192**, 243–250 (2011).
9. F. Jin, B. Dong, J. Georgiou, Q. Jiang, J. Zhang, A. Bharioke, F. Qiu, S. Lommel, M. L. Feltri, L. Wrabetz, J. C. Roder, J. Eyer, X. Chen, A. C. Peterson, K. A. Siminovitch, N-WASp is required for Schwann cell cytoskeletal dynamics, normal myelin gene expression and peripheral nerve myelination. *Development* **138**, 1329–1337 (2011).
10. R. A. Kahn, J. Cherfils, M. Elias, R. C. Lovering, S. Munro, A. Schurmann, Nomenclature for the human Arf family of GTP-binding proteins: ARF, ARL, and SAR proteins. *J. Cell Biol.* **172**, 645–650 (2006).
11. C. D'Souza-Schorey, P. Chavrier, ARF proteins: Roles in membrane traffic and beyond. *Nat. Rev. Mol. Cell Biol.* **7**, 347–358 (2006).
12. J. E. Casanova, Regulation of Arf activation: The Sec7 family of guanine nucleotide exchange factors. *Traffic* **8**, 1476–1485 (2007).
13. J. G. Donaldson, C. L. Jackson, ARF family G proteins and their regulators: Roles in membrane transport, development and disease. *Nat. Rev. Mol. Cell Biol.* **12**, 362–375 (2011).
14. L. Liu, B. Pohajdak, Cloning and sequencing of a human cDNA from cytolytic NK/T cells with homology to yeast *SEC7*. *Biochim. Biophys. Acta* **1132**, 75–78 (1992).
15. E. Meacci, S. C. Tsai, R. Adamik, J. Moss, M. Vaughan, Cytohesin-1, a cytosolic guanine nucleotide-exchange protein for ADP-ribosylation factor. *Proc. Natl. Acad. Sci. U.S.A.* **94**, 1745–1748 (1997).
16. W. Kolanus, W. Nagel, B. Schiller, L. Zeitlmann, S. Godar, H. Stockinger, B. Seed, αLβ2 integrin/LFA-1 binding to ICAM-1 induced by cytohesin-1, a cytoplasmic regulatory molecule. *Cell* **86**, 233–242 (1996).
17. C. Geiger, W. Nagel, T. Boehm, Y. van Kooyk, C. G. Figdor, E. Kremmer, N. Hogg, L. Zeitlmann, H. Dierks, K. S. Weber, W. Kolanus, Cytohesin-1 regulates β-2 integrin-mediated adhesion through both ARF-GEF function and interaction with LFA-1. *EMBO J.* **19**, 2525–2536 (2000).
18. N. Goda, A. Tanoue, S. Kikuchi, G. Tsujimoto, Cloning and characterization of the promoter of murine cytohesin-1 gene. *Biochim. Biophys. Acta* **1493**, 195–199 (2000).
19. T. Hunter, Tyrosine phosphorylation: Thirty years and counting. *Curr. Opin. Cell Biol.* **21**, 140–146 (2009).
20. J. R. Chan, C. Jolicoeur, J. Yamauchi, J. Elliott, J. P. Fawcett, B. K. Ng, M. Cayouette, The polarity protein Par-3 directly interacts with $p75^{NTR}$ to regulate myelination. *Science* **314**, 832–836 (2006).
21. M. Hafner, A. Schmitz, I. Grüne, S. G. Srivatsan, B. Paul, W. Kolanus, T. Quast, E. Kremmer, I. Bauer, M. Famulok, Inhibition of cytohesins by SecinH3 leads to hepatic insulin resistance. *Nature* **444**, 941–944 (2006).
22. B. Fuss, T. Becker, I. Zinke, M. Hoch, The cytohesin Steppke is essential for insulin signalling in *Drosophila*. *Nature* **444**, 945–948 (2006).
23. I. Hofmann, A. Thompson, C. M. Sanderson, S. Munro, The Arl4 family of small G proteins can recruit the cytohesin Arf6 exchange factors to the plasma membrane. *Curr. Biol.* **17**, 711–716 (2007).
24. C. C. Li, T. C. Chiang, T. S. Wu, G. Pacheco-Rodriguez, J. Moss, F. J. Lee, ARL4D recruits cytohesin-2/ARNO to modulate actin remodeling. *Mol. Biol. Cell* **18**, 4420–4437 (2007).
25. S. Hossain, G. Fragoso, W. E. Mushynski, G. Almazan, Regulation of peripheral myelination by Src-like kinases. *Exp. Neurol.* **226**, 47–57 (2010).
26. H. Umemori, S. Sato, T. Yagi, S. Aizawa, T. Yamamoto, Initial events of myelination involve Fyn tyrosine kinase signalling. *Nature* **367**, 572–576 (1994).
27. W. T. Arthur, S. M. Ellerbroek, C. J. Der, K. Burridge, K. Wennerberg, XPLN, a guanine nucleotide exchange factor for RhoA and RhoB, but not RhoC. *J. Biol. Chem.* **277**, 42964–42972 (2002).
28. A. Schmidt, A. Hall, Guanine nucleotide exchange factors for Rho GTPases: Turning on the switch. *Genes Dev.* **16**, 1587–1609 (2002).
29. K. L. Rossman, C. J. Der, J. Sondek, GEF means go: Turning on RHO GTPases with guanine nucleotide-exchange factors. *Nat. Rev. Mol. Cell Biol.* **6**, 167–180 (2005).
30. J. P. DiNitto, A. Delprato, M. T. Gabe Lee, T. C. Cronin, S. Huang, A. Guilherme, M. P. Czech, D. G. Lambright, Structural basis and mechanism of autoregulation in 3-phosphoinositide-dependent Grp1 family Arf GTPase exchange factors. *Mol. Cell* **28**, 569–583 (2007).
31. J. Yamauchi, Y. Miyamoto, H. Hamasaki, A. Sanbe, S. Kusakawa, A. Nakamura, H. Tsumura, M. Maeda, N. Nemoto, K. Kawahara, T. Torii, A. Tanoue, The atypical guanine-nucleotide exchange factor, Dock7, negatively regulates Schwann cell differentiation and myelination. *J. Neurosci.* **31**, 12579–12592 (2011).
32. D. Triolo, G. Dina, I. Lorenzetti, M. Malaguti, P. Morana, U. Del Carro, G. Comi, A. Messing, A. Quattrini, S. C. Previtali, Loss of glial fibrillary acidic protein (GFAP) impairs Schwann cell proliferation and delays nerve regeneration after damage. *J. Cell Sci.* **119**, 3981–3993 (2006).
33. P. V. Monje, J. Soto, K. Bacallao, P. M. Wood, Schwann cell dedifferentiation is independent of mitogenic signaling and uncoupled to proliferation: Role of cAMP and JNK in the maintenance of the differentiated state. *J. Biol. Chem.* **285**, 31024–31036 (2010).

34. X. Liang, N. A. Draghi, M. D. Resh, Signaling from integrins to Fyn to Rho family GTPases regulates morphologic differentiation of oligodendrocytes. *J. Neurosci.* **24**, 7140–7149 (2004).
35. S. S. Scherer, Myelination: Some receptors required. *J. Cell Biol.* **156**, 13–15 (2002).
36. A. Bill, A. Schmitz, B. Albertoni, J. N. Song, L. C. Heukamp, D. Walrafen, F. Thorwirth, P. J. Verveer, S. Zimmer, L. Meffert, A. Schreiber, S. Chatterjee, R. K. Thomas, R. T. Ullrich, T. Lang, M. Famulok, Cytohesins are cytoplasmic ErbB receptor activators. *Cell* **143**, 201–211 (2010).
37. Y. Miyamoto, J. Yamauchi, Cellular signaling of Dock family proteins in neural function. *Cell. Signal.* **22**, 175–182 (2010).
38. B. Aghazadeh, W. E. Lowry, X. Y. Huang, M. K. Rosen, Structural basis for relief of autoinhibition of the Dbl homology domain of proto-oncogene Vav by tyrosine phosphorylation. *Cell* **102**, 625–633 (2000).
39. G. Montagnac, J. B. Sibarita, S. Loubéry, L. Daviet, M. Romao, G. Raposo, P. Chavrier, ARF6 interacts with JIP4 to control a motor switch mechanism regulating endosome traffic in cytokinesis. *Curr. Biol.* **19**, 184–195 (2009).
40. J. Yamauchi, J. R. Chan, E. M. Shooter, Neurotrophins regulate Schwann cell migration by activating divergent signaling pathways dependent on Rho GTPases. *Proc. Natl. Acad. Sci. U.S.A.* **101**, 8774–8779 (2004).
41. T. Torii, Y. Miyamoto, A. Sanbe, K. Nishimura, J. Yamauchi, A. Tanoue, Cytohesin-2/ARNO, through its interaction with focal adhesion adaptor protein paxillin, regulates preadipocyte migration via the downstream activation of Arf6. *J. Biol. Chem.* **285**, 24270–24281 (2010).
42. A. Shevchenko, M. Wilm, O. Vorm, M. Mann, Mass spectrometric sequencing of proteins silver-stained polyacrylamide gels. *Anal. Chem.* **68**, 850–858 (1996).
43. D. Stalder, H. Barelli, R. Gautier, E. Macia, C. L. Jackson, B. Antonny, Kinetic studies of the Arf activator Arno on model membranes in the presence of Arf effectors suggest control by a positive feedback loop. *J. Biol. Chem.* **286**, 3873–3883 (2011).
44. A. Tanoue, S. Ito, K. Honda, S. Oshikawa, Y. Kitagawa, T. A. Koshimizu, T. Mori, G. Tsujimoto, The vasopressin V1b receptor critically regulates hypothalamic-pituitary-adrenal axis activity under both stress and resting conditions. *J. Clin. Invest.* **113**, 302–309 (2004).
45. Y. Matsuda, V. M. Chapman, Application of fluorescence in situ hybridization in genome analysis of the mouse. *Electrophoresis* **16**, 261–272 (1995).

Acknowledgments: We thank E. M. Shooter and Y. Kaziro for their participation in insightful discussions. **Funding:** This work was supported by Grants-in-Aid for Scientific Research from the Ministry of Education, Culture, Sports, Science and Technology (MEXT) (22300123 and 23650200 to J.Y.) and the Ministry of Health, Labour and Welfare (MHLW) (KHA1001, KHA1202, and 24-18 to J.Y.) and partially by research grants from the Takeda Foundation (to J.Y. and Y.M.) and the Uehara Foundation (to J.Y. and Y.M.). **Author contributions:** J.Y. designed the experiments; J.Y., Y.M., and T.T. performed the production of antibodies, construction of plasmids, transfection experiments, Western blotting analysis, immunoprecipitations, biochemical assays, and immunofluorescence and immunohistochemistry experiments; J.Y. generated the transgenic mice; Y.M. performed the in vitro myelination experiments; T.T. performed the protein purification and binding assays; J.Y., Y.M., T.T., S.T., and J.R.C. made the figures; J.Y. and J.R.C. wrote the paper; K. Kondo performed the molecular modeling; K. Kawahara and N.N. performed the EM analysis; and G.T. and A.T generated the knockout mice. **Competing interests:** The authors declare that they have no competing interests.

Submitted 27 December 2011
Accepted 7 September 2012
Final Publication 25 September 2012
10.1126/scisignal.2002802
Citation: J. Yamauchi, Y. Miyamoto, T. Torii, S. Takashima, K. Kondo, K. Kawahara, N. Nemoto, J. R. Chan, G. Tsujimoto, A. Tanoue, Phosphorylation of cytohesin-1 by Fyn is required for initiation of myelination and the extent of myelination during development. *Sci. Signal.* **5**, ra69 (2012).

J Phys Fitness Sports Med, **1(2)**: 263-269 (2012)

JPFSM: ***Review Article***

Neural control of human gait and posture

Kimitaka Nakazawa, Hiroki Obata and Shun Sasagawa

Department of Life Sciences, Graduate School of Arts and Sciences, The University of Tokyo, 3-8-1 Komaba, Meguro-Ku, Tokyo 153-8902, Japan

Received: April 21, 2012 / Accepted: June 12, 2012

Published by
The Japanese Society of Physical Fitness and Sports Medicine